

Facies analysis, sequence stratigraphy, and carbon isotope chemostratigraphy of a classic Zn-Pb host succession: The Proterozoic middle McArthur Group, McArthur Basin, Australia



Marcus Kunzmann^{a,b,*}, Susanne Schmid^a, Teagan N. Blaikie^{a,b}, Galen P. Halverson^{c,d}

^a CSIRO Mineral Resources, Australian Resources Research Centre, Kensington, WA 6151, Australia

^b Northern Territory Geological Survey, Darwin, NT 0800, Australia

^c Dept. of Earth & Planetary Sciences/Geotop, McGill University, Montréal, Québec, Canada

^d Earth Dynamics Research Group, The Institute for Geoscience Research (TIGeR), School of Earth and Planetary Sciences, Curtin University, GPO Box U1987, WA 6845, Australia

ARTICLE INFO

Keywords:

McArthur Basin
Barney Creek Formation
Zn-Pb deposits
Chemostratigraphy
Sequence stratigraphy
Mineral exploration under cover

ABSTRACT

The McArthur Basin is part of a Proterozoic basin system on the North Australian Craton that represents a world-class Zn-Pb province. Ore bodies are typically stratiform and hosted by pyritic, organic-rich, and dolomitic siltstones deposited in local depocenters and sub-basins. The mineralization is characterized by syngenetic and/or diagenetic textures. These characteristics highlight the need to understand the sedimentological and structural evolution of the basin for mineral exploration. Here we report a facies analysis of the middle McArthur Group (Tooganinie to Lynott formations) in the southern McArthur Basin, distinguishing four facies associations and 19 lithofacies. Depositional environments range from slope and deep subtidal settings to supratidal sabkhas. The middle McArthur Group records a systematic $\sim 3.5\%$ shift in the carbon isotope ratio of carbonates ($\delta^{13}\text{C}_{\text{carb}}$) that can likely be used for basin-wide or even global correlation. The Barney Creek Formation, the main Zn-Pb host unit, was mostly deposited under deep subtidal to slope conditions, although shoaling to shallow subtidal environments locally occurred on paleohighs. Together with the overlying Reward Dolostone, it comprises two 3rd-order transgressive-regressive sequences, which distinguishes it from the younger and less prospective but lithologically similar Caranbirini Member, which only comprises one incomplete sequence. The HYC Pyritic Shale Member of the lower Barney Creek Formation, which hosts most of the known mineralization, is lithologically similar across the studied area, and reflects significant deepening of the entire basin. A maximum flooding surface in the HYC Pyritic Shale Member represents the most pyritic and organic-rich interval and can be developed as a black shale in sub-basin depocenters. It represents an ideal chemical trap for base metals in syngenetic models for mineralization; however, lithification and compaction would convert this black shale interval into a physical trap in diagenetic models. Regardless of the preferred model, sequence stratigraphy integrated with facies maps can be used for targeting.

1. Introduction

Mineral exploration for stratiform ore deposits in sedimentary basins requires a detailed understanding of the architecture and evolution of the basin fill. Among the first steps to evaluate the prospectivity of the sedimentary succession is to evaluate the depositional environments of individual stratigraphic units and construct a stratigraphic framework. In Phanerozoic basins, sequence and lithostratigraphy are usually supported by biostratigraphy and geochronology to formulate a coherent chronostratigraphy. The limited applicability of biostratigraphy

in Precambrian basins motivates the application of chemostratigraphy, in particular the carbon isotope composition of inorganic carbon (e.g., Halverson et al., 2005, 2010), to bolster other stratigraphic data sets. The constructed stratigraphic framework can then be used in conjunction with structural information to reconstruct basin architecture, for example the distribution of paleohighs and sub-basins. In the search for sediment-hosted massive Zn-Pb deposits in the McArthur Basin of northern Australia, a detailed understanding of sub-basins is vital as carbonaceous, pyritic mudstones deposited in sub-basins host the most significant mineralization (e.g., McGoldrick et al., 2010). This also

* Corresponding author.

E-mail address: marcus.kunzmann@csiro.au (M. Kunzmann).

<https://doi.org/10.1016/j.oregeorev.2019.01.011>

Received 28 June 2018; Received in revised form 19 December 2018; Accepted 15 January 2019

Available online 22 January 2019

0169-1368/ © 2019 Commonwealth Scientific and Industrial Research Organization. Published by Elsevier B.V. This is an open access article under the CC BY license (<http://creativecommons.org/licenses/by/4.0/>).

highlights the importance of sequence stratigraphy to predict where in the sub-basin the most prospective mudstones occur.

The late Paleo- to early Mesoproterozoic McArthur Basin in the Northern Territory of Australia contains a ~5–15 km-thick mixed siliciclastic-carbonate succession with bimodal volcanics near the base (e.g., Plumb, 1979a,b; Jackson et al., 1987; Rawlings, 1999). Together with the Isa Superbasin in Queensland, its southeastern continuation, it represents one of the most prospective Zn-Pb-Ag provinces in the world (e.g., Leach et al., 2005, 2010; Huston et al., 2006). For example, dolomitic siltstones and shales of the ca. 1640 Ma Barney Creek Formation in the southern McArthur Basin host the world-class McArthur River deposit (e.g., Smith and Croxford, 1973, 1975; Croxford, 1975; Williams and Rye, 1974; Williams, 1978; Eldridge et al., 1992; Large et al., 1998; Logan et al., 2001; Chen et al., 2003; Ireland et al., 2004a,b; Symons, 2006; Holman et al., 2014). In addition, the Barney Creek Formation is one of the oldest active petroleum systems in the world and may be an important hydrocarbon source unit and unconventional reservoir (Jackson et al., 1986, 1988; Crick et al., 1988; Summons et al., 1988; Baruch et al., 2015).

Despite its economic importance, only a few sedimentological and stratigraphic studies of the Barney Creek Formation and over- and underlying stratigraphic units (i.e., middle McArthur Group) are available in the literature (Brown et al., 1978; Jackson et al., 1987; Bull, 1998; McGoldrick et al., 2010). In this contribution to the special issue, we present a detailed facies analysis of the middle McArthur Group in the southern McArthur Basin. As our facies analysis is based on exploration drill cores, which is what exploration geologists mostly work with in this area, our rock descriptions and interpretations of the depositional environments can directly be applied to new drill cores. We use our facies analysis to provide a lithostratigraphic and sequence stratigraphic interpretation of this succession. Furthermore, we tie a high-

resolution carbon isotope record into our stratigraphic framework and test its applicability for future basin-wide and global stratigraphic correlation.

2. Regional geology

The greater McArthur Basin (Fig. 1A) is part of a large Proterozoic basin system on the North Australian Craton (e.g., Scott et al., 2000; Giles et al., 2002; Betts et al., 2003; Betts and Giles, 2006; Selway et al., 2009; Gibson et al., 2017). It is bounded by older Paleoproterozoic basement of the Pine Creek Inlier in the northwest, the Arnhem Inlier in the north, and the Murphy Inlier in the southeast (Fig. 1A). Its westernmost exposure occurs in the Birrindudu Basin along the Northern Territory-Western Australia border. Elsewhere, the basin extends under younger sedimentary cover or the Gulf of Carpentaria. The McArthur Basin is divided into the northern McArthur and southern McArthur basins, separated by the east-west striking Urupunga Fault Zone. The most important structural features are the Walker and Batten Fault Zones in the northern and southern McArthur Basin respectively (Fig. 1A, B). These structurally complex fault zones are north-south striking corridors, each about 80 km wide and 200 km long. They were initially interpreted to represent asymmetric half-grabens in which sediment thickness significantly exceeds those in adjacent areas (e.g., Plumb, 1979a; Plumb and Wellman, 1987). However, a seismic reflection survey in the southern McArthur Basin failed to confirm a graben-like depocenter (Rawlings et al., 2004). Instead, the seismic data suggest that the middle McArthur Group was deposited in a gently east-dipping ramp setting, characterized by small-scale sub-basins that opened along the Emu Fault in the Batten Fault Zone (Fig. 1B; Rawlings et al., 2004).

The ca. 1670–1600 Ma McArthur Group is exposed in the southern

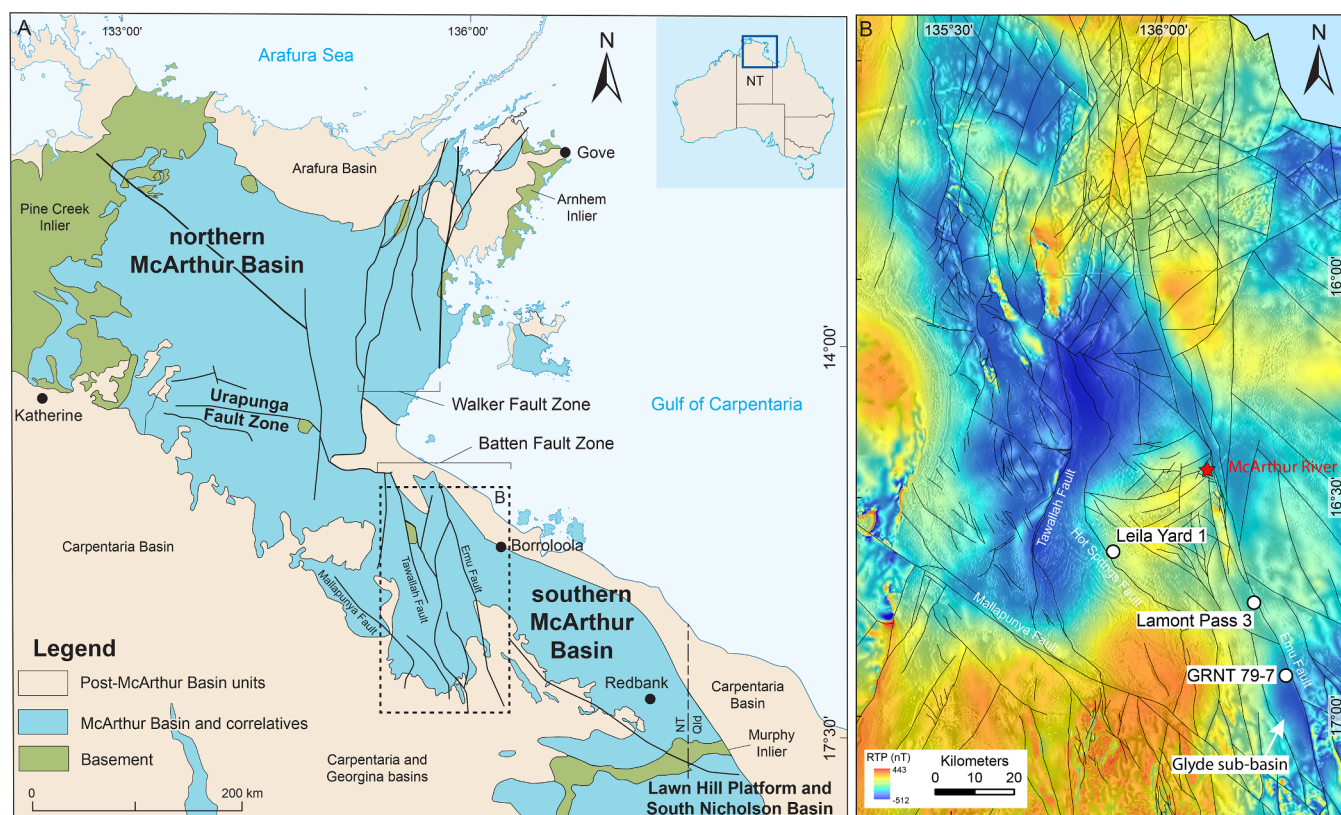


Fig. 1. Simplified geological map of the McArthur Basin and magnetics of the Batten Fault Zone. A) Geographical distribution of McArthur Basin and equivalent stratigraphy, as well as basement inliers and younger sedimentary cover (modified from Ahmad et al. (2013)). B) Reduced to pole magnetics overlaid on the tilt-derivative of the Batten Fault Zone (inset in A) highlighting the current structural complexity of the basin (modified from Blaikie and Kunzmann, 2018). Also shown are the location of the McArthur River deposit and studied drill cores.

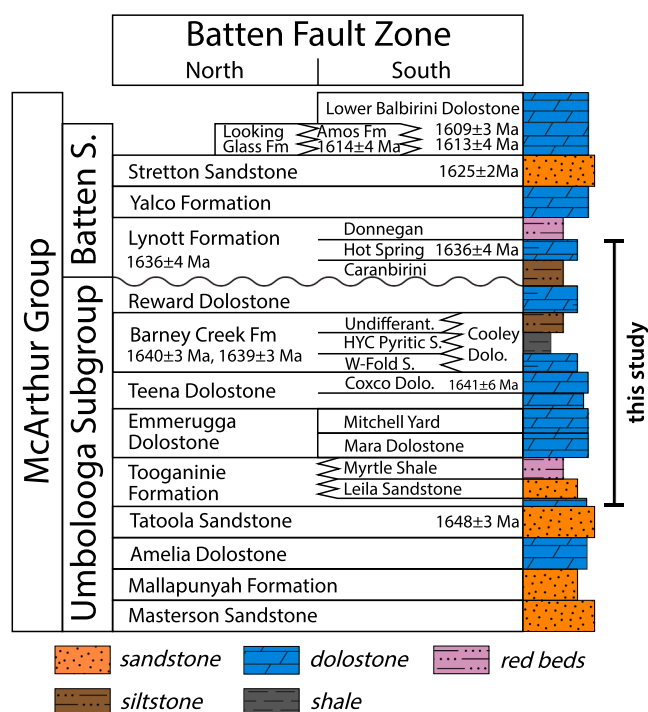


Fig. 2. Stratigraphy, dominant lithology, and geochronological constraints of the McArthur Group. Stratigraphy modified from Ahmad et al. (2013), radiometric ages from Page and Sweet (1998) and Page et al. (2000).

McArthur Basin and reaches a thickness of 1–3.5 km (Jackson et al., 1987; Rawlings, 1999; Rawlings et al., 2004). The McArthur Group is subdivided into the Umbloolga and Batten Subgroups, separated by a local unconformity at the top of the Reward Dolostone (Fig. 2; Jackson et al., 1987). This contribution focuses on the middle McArthur Group, i.e. from the Tooganinie Formation to the middle Lynott Formation (Fig. 2).

The ca. 200 m-thick Tooganinie Formation conformably overlies the Tatoola Sandstone (Fig. 2). It is dominated by dololite, stromatolites (including *Conophyton*), dolarenite, oolites, and dolomitic siltstone and shale. Regular interbedding of dolostone and siliciclastic beds is a characteristic feature of the Tooganinie Formation (Jackson et al., 1987). Evidence for exposure include mudcracks, halite casts, gypsum pseudomorphs, and tepees. The inferred depositional environment encompasses peritidal lagoon and shoal complexes in the southern Batten Fault Zone, which transition into sabkha and terrestrial environments to the north (Jackson et al., 1987).

The < 10–30 m thick Leila Sandstone is composed of sandstone and dolomitic sandstone and conformably overlies the Tooganinie Formation (Jackson et al., 1987). Cross-bedding, mudcracks, and intraclasts are common. This unit was likely deposited in shallow subtidal to emergent environments (Jackson et al., 1987).

The Emmerugga Dolostone is up to 620 m thick and is subdivided into the Mara Dolostone and Mitchell Yard members in the southern Batten Fault Zone (Fig. 2; Plumb and Brown, 1973). The Mara Dolostone consists of stromatolitic dolostone (with prominent *Conophyton*), dolarenite, and dololite with occasional halite casts. The dolostones are arranged in shallowing-upward cycles and were deposited in shallow subtidal to intertidal environments (Brown et al., 1978; Ahmad et al., 2013). The Mitchell Yard Member is composed of heavily altered dololite. Therefore, inferred depositional environments for this member span a wide range from deep subtidal to supratidal (Brown et al., 1978; Jackson et al., 1987; Ahmad et al., 2013).

The Teena Dolostone conformably overlies the Emmerugga Dolostone and is subdivided into a lower unnamed member and the

upper Coxco Dolostone Member (Fig. 2; Jackson et al., 1987). The lower member is up to 60 m thick and mainly consists of dololite, stromatolitic dolostone, and cross-laminated dolarenite deposited in shallow subtidal to intertidal (Brown et al., 1978; Ahmad et al., 2013) or supratidal environments (Jackson et al., 1987). The Coxco Dolostone Member is up to 70 m thick and is characterized by dololite and minor stromatolitic dolostone. The most striking feature of this unit are radiating fans of near-vertical to vertical, acicular, mm to <10 cm large ‘Coxco needles’. These needles have been variably interpreted as gypsum pseudomorphs (Walker et al., 1977), lacustrine trona (Jackson et al., 1987), and seafloor aragonite cement (Brown et al., 1978; Winefield, 2000). A tuff bed in the Coxco Dolostone Member yielded a U-Pb SHRIMP age of 1639 ± 6 Ma (Page et al., 2000).

The transition to the overlying Barney Creek Formation was accompanied by a change in the tectonic regime in the southern McArthur Basin, and likely led to formation of local unconformities (cf. Walker et al., 1983). The depositional setting changed from a stable shallow marine platform, likely with inherited relief, to a compartmentalized basin with numerous paleohighs and sub-basins (McGoldrick et al., 2010). Sub-basin formation was related to a sinistral strike-slip regime of arcuate and broadly N-S trending fault systems (Emu, Tawallah, and Hot Springs faults; Fig. 1B). Whereas transpression occurred at E to N trending segments of the faults, transtension along N to NW trending segments created accommodation space and led to opening of sub-basins (McGoldrick et al., 2010). Although these structures were later inverted, they must have had a major control on the deposition of the Barney Creek Formation and the overlying Reward Dolostone as indicated by significant lateral facies and thickness changes within these units (Brown et al., 1978; Jackson et al., 1987; McGoldrick et al., 2010).

The 10–900 m-thick Barney Creek Formation comprises three members: the W-Fold Shale, the HYC Pyritic Shale, and the Cooley Dolostone (Jackson et al., 1987). These members are overlain by the undifferentiated upper part of the formation (Fig. 2). All three members were defined in the HYC (‘Here’s Your Chance’) sub-basin that hosts the McArthur River (HYC) deposit and partly represent lateral facies changes instead of basin-wide lithostratigraphic units (Jackson et al., 1987). This is particularly important for the Cooley Dolostone, which only occurs along local fault scarps. The W-Fold Shale represents the basal member of the Barney Creek Formation and consists of green and red dolomitic siltstone or pink dololite (Brown et al., 1978; Jackson et al., 1987; Davidson and Dashlooty, 1993). The following HYC Pyritic Shale Member, which hosts the McArthur River Zn-Pb-Ag deposit, consists of dolomitic and pyritic siltstones and minor silty shales. Formerly interpreted to record deposition in a shallow marine or lacustrine setting (cf. Jackson et al., 1987), the HYC Pyritic Shale Member is now generally regarded to have formed in a deep subtidal environment (Bull, 1998; Winefield, 1999). Three tuff beds from the HYC Pyritic Shale Member yielded U-Pb SHRIMP ages of 1638 ± 7 Ma, 1639 ± 3 Ma, and 1640 ± 3 Ma (Page and Sweet, 1998). The Cooley Dolostone Member is a carbonate breccia related to faults and mass flows that interfingers with the other members of the Barney Creek Formation (Jackson et al., 1987; Ahmad et al., 2013). The clasts are mostly sourced from the Emmerugga and Teena dolostones (Brown et al., 1978; Ahmad et al., 2013). The upper undifferentiated part of the Barney Creek Formation consists of dolomitic siltstone and dolarenite (e.g., Jackson et al., 1987).

The up to 350 m-thick Reward Dolostone conformably overlies the Barney Creek Formation and mostly consists of dololite, dolarenite, stromatolitic dolostone, and dolomitic sandstone, deposited in shallow subtidal to peritidal environments (Brown et al., 1978; Jackson et al., 1987). It is characterized by sharp lateral thickness and facies changes (Jackson et al., 1987).

The contact with the overlying Lynott Formation is variably transitional or unconformable (Jackson et al., 1987; Ahmad et al., 2013; Walker et al., 1983). This contact represents the boundary between the Umbloolga and Batten subgroups (Fig. 2) and the end of the major

transgressive-regressive cycle that started with the deposition of the lower Emmerugga Dolostone. The Lynott Formation comprises the up to 400 m thick Caranbirini, up to 350 m thick Hot Spring, and up to 134 m thick Donnegan members (Jackson et al., 1987). The Caranbirini Member shares lithological similarities with the Barney Creek Formation as it is composed of dolomitic and partly pyritic siltstone and shale. The rocks were likely deposited in deep subtidal environments. The overlying Hot Spring Member represents shoaling and mostly consists of stromatolitic dolostone, cross-laminated dolarenite, and dololite with common evaporite pseudomorphs. This unit was deposited in peritidal environments (Jackson et al., 1987; Ahmad et al., 2013). A tuff bed in the Hot Spring Member was dated at 1636 ± 4 Ma by U-Pb SHRIMP analysis (Page et al., 2000). Further shallowing-upward led to deposition of purple-brown dolomitic siltstones and sandstones, and silicified stromatolitic dolostone and dolarenite of the Donnegan Member. This unit was deposited in peritidal to supratidal sabkha environments (Jackson et al., 1987; Ahmad et al., 2013).

2.1. Zn-Pb-Ag deposits in the McArthur Basin

The only mined stratiform sediment-hosted Zn-Pb-Ag deposit in the McArthur Basin is the McArthur River deposit (Fig. 1B). It is by far the largest zinc resource in this basin with a pre-mining estimate of 227 Mt at 9.2% Zn, 4.1% Pb, 41 g/t Ag, and 0.2% Cu (Logan et al., 1990). The mineralization is hosted by the HYC Pyritic Shale Member in the HYC sub-basin, which is ca. 1–2 km \times 5 km large and bounded to the east by the Western Fault of the Emu Fault system (e.g., Porter, 2017). Timing of the mineralization is debated but generally thought to be syngenetic to diagenetic (e.g., Eldridge et al., 1992; Large et al., 1998; Ireland et al., 2004a,b).

The stratiform sediment-hosted Teena Zn-Pb deposit is located in the Teena sub-basin, 8 km to the west of the McArthur River deposit and has a resource estimate of 58 Mt at 11.1% Zn and 1.6% Pb (Taylor et al., 2017). Two stratiform ore bodies, separated by a siliciclastic mass-flow deposit, are hosted by the HYC Pyritic Shale Member and occur at a depth between 600 and 1000 m for more than 1.5 km along strike (Taylor et al., 2017). The mineralization is interpreted as early diagenetic (Taylor et al., 2017).

Other sediment-hosted Zn-Pb deposits in the McArthur Basin include the Cooley and Ridge deposits, a group of small deposits located immediately east of McArthur River (Williams, 1978). Here, the HYC Pyritic Shale Member is only mineralized in the western portion of the Ridge II deposit. The ore occurs ca. 300 m stratigraphically above the mineralization at the McArthur River deposit. The bulk of the mineralization is epigenetic and hosted by carbonate breccias of the Emmerugga Dolostone (Cooley deposits) or Cooley Dolostone Member (Ridge deposits) of the Barney Creek Formation (Williams, 1978). Carbonate-hosted Zn-Pb mineralization also occurs at the Coxco deposit, comprising two prospects located ca. 10 km southeast of McArthur River (Walker et al., 1983). Epigenetic mineralization occurs in karst cavities and breccias within the Mara Dolostone Member of the Emmerugga Dolostone and the Reward Dolostone, separated by a karst surface. The W-Fold and Mitchell Yard sub-basins, ca. 5 km to the west and 6 km to the southwest of McArthur River respectively, host weak stratiform mineralization in the HYC Pyritic Shale Member (e.g., Lambert and Scott, 1973). Furthermore, weak stratiform and breccia-hosted Zn mineralization has also been reported from the ca. 1730 Ma McDermott and Wollongorang formations of the Tawallah Group (Spinks et al., 2016).

3. Methods

In this paper we present a detailed facies analysis of stratigraphic units comprising the middle McArthur Group. We then use this sedimentological evaluation for a sequence stratigraphic interpretation. Furthermore, high-resolution carbon isotope chemostratigraphic

records are integrated into this sequence stratigraphic framework to test its applicability in the McArthur Basin. All facies data are summarized in Table 1 and all carbon and oxygen isotope ratios are provided in Supplementary Table 1.

3.1. Facies analysis

Facies analysis is based on decimetre scale logs of 16 drill cores. However, a presentation of all core data is beyond the scope of this paper. Therefore, only three drill core logs are presented herein, which were chosen to represent as much stratigraphy as possible, as well as sub-basin and paleohigh settings. Facies associations and lithofacies were distinguished based on compositional and textural properties, and the occurrence of distinct sedimentary structures. Petrographic analysis of polished thin sections supported the facies analysis.

3.2. Sequence stratigraphy

We defined third-order transgressive-regressive (T-R) sequences following the convention of Embry (1993, 2009) and Embry and Johannessen (2017). T-R sequences are divided into a transgressive systems tract (TST), formed during base level rise, and a regressive systems tract, formed during base level fall. Therefore, sequences are bound by subaerial unconformities or unconformable shoreline ravinement surfaces on the flanks of the basin, and maximum regressive surfaces (MRS) in more basinal settings. The TST and RST are separated by the maximum flooding surface (MFS). We identified sequence stratigraphic surfaces by a combination of facies data and available gamma logs. The gamma log records the radioactivity of naturally-occurring uranium, thorium, and potassium. These elements are common in clays and thus, an increase in radioactivity corresponds to an increase in clay content (i.e., shale). Generally speaking, an increase in shale marks the deepening of the depositional environment in siliciclastic systems. In mixed siliciclastic-carbonate systems, it is important to complement gamma ray interpretations with facies analysis as flooding can be manifested in the deposition of carbonate facies with potentially weaker radioactivity. An example would be the flooding of a siliciclastic sabkha environment and deposition of marine carbonates. In addition to facies data and gamma logs, our sequence stratigraphic interpretation was also supported by carbon isotope chemostratigraphy as we identified systematic shifts in the $\delta^{13}\text{C}_{\text{carb}}$ curve associated with some sequence boundaries and MFS.

3.3. Carbon and oxygen isotopes

The carbon isotopic composition of dissolved inorganic carbon (DIC) in seawater varies secularly (e.g., Saltzman and Thomas, 2012). This feature in the carbon isotope record is commonly used to correlate carbonate rocks based on their isotopic composition because the precipitation of carbonate involves little isotopic fractionation (e.g., Maslin and Swann, 2005). Photosynthesis preferentially consumes the light isotope of C (^{12}C), which leads to depletion of organic matter in the heavy isotope (^{13}C). The isotopic composition of DIC thus reflects the partitioning of carbon between the organic carbon and carbonate carbon reservoirs (e.g., Kump and Arthur, 1999). Considering that the residence time of carbon in the modern ocean (ca. 100 kyr; de la Rocha, 2006) is about two orders of magnitude longer than the mixing time of the ocean (ca. 1000 years; de la Rocha, 2006), coeval carbonate rocks in one basin, and even globally, can have the same isotopic composition. Apart from the composition of the global DIC, local processes can influence the isotopic composition of local water masses and carbonate rocks that precipitate from them. The biological pump produces a surface-to-depth isotope gradient. Primary productivity leads to a ^{12}C -depleted surface ocean through biological assimilation and a ^{12}C -enriched deep ocean through remineralization of organic matter (e.g., Sarmiento and Gruber, 2006). The magnitude of this gradient depends

Table 1
Detailed description of lithofacies from the middle McArthur Group.

Lithofacies	Composition	Sedimentary Structures	Depositional Environment	Distribution
FA1: Supratidal to continental LF1: Red or green siltstone	Siltstone and clay-rich siltstone, rare claystone; partly dolomitic; green or red	Laminated to massive; anhydrite nodules (often displacing laminae) and veins; chicken wire; mudcracks; common mm-scale to <10 cm thick, continuous or discontinuous sandstone (LF2) laminae/beds/channels with siltstone and dolostone intraclasts; flame and ball-and-pillow structures; occasional starved ripples; sometimes oxidation/reduction spots/texture	Upper intertidal to supratidal sabkha environments; green variety more submerged environments, i.e. more seaward and/or in creeks and ponds	Tooganinie Fm, Myrtle Shale
LF2: Sandstone	Quartz arenite and subarkose; pink or medium to dark grey/green; sometimes silty or dolomitic; very fine to coarse; subangular to well rounded; poorly to well sorted; immature; rare conglomerate interbeds with granules	Thickly laminated to thinly bedded; mudcracks; occasional anhydrite nodules and veins; red and green siltstone intraclasts (sub-angular to rounded; circular and tabular); occasional cross-lamination; scouring; occasional fining-upward	Supratidal sabkha to peritidal; deposition during episodic flooding (sheet flood?) events possible	Leila Sandstone, Myrtle Shale
LF3: Conglomerate	Clast-supported; grey to brown; polymict (siltstone (LF1), sandstone (LF2), and dolostone clasts), granules to boulders, sub-rounded to very well rounded; sometimes silica cement; occasional siltstone (LF3) interbeds	Thickly laminated to very thinly bedded; erosional base	Intertidal to supratidal (sabkha); comparable to LF2	W-Fold Shale; Myrtle Shale
FA2: Shallow subtidal to intertidal LF4: Bedded dolarenite	Light to medium grey, rarely dark grey; dolosiltite to dolarenite (mostly very fine but up to coarse), rare dolorudite; silification possible; occasional floating quartz (sand to granules, well rounded) or interbeds of marine sandstone (LF5) and marine siltstone (LF6); pyrite and organic matter streaks common when interbedded with dolomudstone; base metals may occur when brecciated	Thickly laminated to medium bedded, sometimes massive; typically parallel-planar laminated/bedded but occasional nodular bedding, carbonate nodules, wavy and/or discontinuous shale or siltstone laminae, or cross lamination; laminae/beds/channels of same facies or marine sandstone (LF5) with (low-angle) cross lamination; individual beds or bed sets fining-upward; scouring common; rare silicified or calcite-filled fenestrae; rip-ups, mud chips, and discrete intraclast beds (tempestites?); soft-sediment deformation, loading and ball-and-pillow structures may occur; sand-filled mudcracks and anhydrite veins common when interbedded with FA1; rare radiating acicular pseudomorphs; sometimes molar tooth structures when interbedded with muddy microbialaminite; can host brecciated and silicified exposure surfaces	Deposition in complex mosaic of shallow subtidal to upper intertidal, occasionally even supratidal environments such as shoals, lagoons, beaches, beach ridges, tidal channels, levee crests, tidal channel bars, ponds; occasional storm events and/or strong tidal currents	All units
LF5: Marine sandstone	Light to medium grey (rare dark grey) quartz arenite; medium to coarse grained; rounded to well rounded; well sorted; may contain well rounded carbonate grains, carbonate matrix (sometimes silicified); continuum with bedded dolarenite containing floating quartz; interbeds of bedded dolarenite (LF4) and other facies from FA1, FA2; some pyrite, either disseminated or in spots	Massive; may contain tabular, mm- to cm-scale rip-up clasts of bedded dolarenite (LF4)	Shallow subtidal to intertidal environments, occasional storm events and/or strong tidal currents	Myrtle Shale; Hot Spring Mbr
LF6: Marine siltstone	Dark grey/green to black siltstone; partly dolomitic; occasional interbeds of FA1, FA2; sometimes pyrite	Thickly laminated; planar-parallel to wavy lamination; discontinuous or continuous laminae, beds, or channels of LF4 with uni- or bidirectional cross-lamination; starved ripples; rare mudcracks; synaeresis cracks; occasional ball-and-pillow structures	Shallow subtidal to upper intertidal; less hydrodynamic energy than LF5; tidal current- and storm-influenced	Tooganinie Fm
LF7: Microbialaminite	Light to medium grey (rare dark grey) doloboundstone; commonly silicified; floating quartz possible; interbedded with FA2, follows LF11 (FA3) in shoaling-up cycles	Centimeter- to meter-thick microbialaminite; mm-scale flat, crinkly, and undulating lamination; irregular, < 5 mm high domal structures; occasional fenestrae, tepees, and mudcracks; discrete intervals of intraclast breccias; sometimes vuggy or brecciated	Low-energy inter- to lower supratidal environments (e.g., intertidal flats, levee crests)	All units

(continued on next page)

Table 1 (continued)

Lithofacies	Composition	Sedimentary Structures	Depositional Environment	Distribution
LF8: Dololite	Light grey to pink, rarely medium grey dololite/micrite; interbedded with FA2 and LF11 of FA3	Thinly laminated to massive; common silicified fenestrae; common acicular, radiating, mm- to cm-scale pseudomorphs in pink dololite; silicified karst surfaces may occur; rare mudcracks filled with LF4; sometimes channels and continuous or discontinuous laminae (scoured bases) of LF4 (cross-lamination, starved ripples, fining-upward); LF4 intracasts (often silicified)	Deposition in complex mosaic of shallow sub- to lower supratidal environments such as protected lagoons and platforms; on the lee side of banks, shoals, and stromatolite build-ups; on levee crests; ponds; and low-energy parts of tidal channels; storm and tidal activity	All units
LF9: Interbedded dolarenite with red, green, or brown siltstone laminae	Light grey to pink dololite, dolosiltite, or dolarenite intervals alternate with red, green, or brown siltstone or shale laminae (continuous or discontinuous, < 10 mm thick)	Very thinly bedded; wavy, continuous or discontinuous bedding; occasional acicular and radiating pseudomorphs; intracasts and mud chips; some flame structures; some scour structures	Deposition in facies mosaic of shallow subtidal (carbonate laminae and beds) to lower intertidal environments; siliciclastic component deposited in intertidal ponds close to fluvial/estuarine source; storm and tidal activity	W-Fold Shale
FA3: Subtidal LF10: Ooid grainstone	Medium grey dolopackstone or dolograinstone; ooids (aggregation possible); silicified, interbedded with FA1, FA2, FA3	Massive; rip-up clasts of bedded dolarenite (LF4) and dololite (LF8)	High-energy shallow subtidal bars and shoals; beach environments also possible	Tooganinie Fm
LF11: Stromatolite	Medium grey (rare black) doloboundstone; occasionally silicified and brecciated; interbedded with FA1, FA2, FA3	Decimeter-scale domal or columnar (laterally linked) with synoptic relief of <10 cm (potentially larger), rare <i>Conophyton</i> ; often grow of brecciated surfaces and are brecciated at top, or entire interval brecciated; intraclast beds or micritic fill between domes	Shallow sub- to intertidal environments characterized by high wave and tidal energy such as headlands; bioherms and biostroms possible; may have formed barrier complexes	All units
LF12: Muddy microbialaminite	Dark grey to black doloboundstone; clay-rich; rarely silicified; sometimes fine-grained pyrite along laminae; interbedded with FA2, FA3	Flat, crinkly, and undulating lamination; occasional disrupted and buckled laminae; common molar tooth structure; rare fenestrae (laminoid, calcite-filled, 1 mm high and 5–10 mm long)	Quiet shallow subtidal environments with low wave and tidal energy such as bights, lagoons, and embayments	Reward Dolostone; Lynott Fm
LF13: Dolomudstone	Dark grey to black (minor medium grey) homogeneous dololite to dolosiltite; clay-rich; sometimes silty (quartz); pyrite and base metals may occur disseminated, stratiform, in streaks, spots, or along fractures; interbeds of muddy microbialaminite (LF12) or back shale (LF17) possible; can transition into dololite (LF8)	Thinly laminated to massive; nodular bedding and pale grey nodules (can be plastically deformed) may occur; flakes of organic matter (<1 cm, subhorizontal); slumping, loading, ball-and-pillow structures may occur; molar tooth structures possible; rare dolarenite laminae with cross-lamination or starved ripples; rip-up clasts (dolarenite) possible; discontinuous or wavy shale laminae may occur; partly flake breccia (pale grey clasts, subangular to rounded; mostly tabular, matrix supported; clasts subhorizontal)	Quiet subtidal environments above storm wave base; similar to LF12 by algae growth prevented by higher sedimentation rates or greater water depth	Barney Creek Fm; Reward Dolostone; Lynott Fm
FA4: Deep subtidal to slope LF14: Dolarenite	Mostly medium grey dolosiltite to dolarenite (mostly very fine- to fine-grained arenite); may be silty or contain rounded quartz grains; disseminated or accumulations of pyrite may occur; interbedded with LF15, LF16, LF18; poorly to well sorted	Thinly laminated to medium bedded; may have cross-lamination, starved ripples, HCS; fining- or coarsening-upward possible; often sharp and scouring base but transitional top; slumping possible; loading and ball-and-pillow structures into underlying facies common; may have mm to cm scale intracasts (LF4, LF11, LF16, rounded); sub-mm to mm scale organic matter flakes are common, may be disseminated, concentrated in certain beds or form discontinuous laminae	Deposition from sediment-gravity flows such as grainflows and turbidity currents in deep subtidal slope environments; some beds likely storm deposits around storm wave base	Barney Creek Fm
LF15: Interbedded dolarenite with grey siltstone	Medium grey dolosiltite and dolarenite (floating quartz possible) interbedded with dolomitic siltstone of LF 16; >50% dolosiltite/dolarenite; generally cm-scale alteration, sometimes 10–20 cm scale alteration; often interbedded and continuous with LF16	Thickly laminated to very thinly bedded; dolarenite beds scour siltstone laminae; loading, flame, and ball-and-pillow structures common; occasional slumping and growth faults; mud chips and organic matter flakes; dolarenite beds can have cross-lamination, SCS and starved ripples; occasional carbonate nodules	As LF14, deposition from sediment gravity flows; difference is thinner but regularly occurring beds	Barney Creek Fm
LF16: Silty dolarenite/dolomitic siltstone	Continuum between medium to dark grey silty dolostone and dark grey to black dolomitic siltstone/very fine sandstone (both brown or white/rusty)	Thickly laminated to thinly bedded; generally parallel-planar lamination, occasional wavy lamination; occasional carbonate nodules, slumping, growth faults,	Dolomitic siltstone subfacies below storm wave base, silty dolarenite in shallower environments close to storm wave base; both deposition from	Barney Creek Fm, Caranbirini Mbr

(continued on next page)

Table 1 (continued)

Lithofacies	Composition	Sedimentary Structures	Depositional Environment	Distribution
LF17: Black Shale	weathering); siltstone often pyritic and/or bituminous; occasional dolarenite laminae and beds (LF14, LF15); interbeds of other FA4 lithofacies common	fining upward; common loading structures associated with dolarenite laminae; often fissile breaking when interbedded with black shale (LF17); silty dolarenite very rare cross-lamination (tangential or straight foresets), starved ripples, HCS Parallel-planar laminated; fissile or rubbly	hemipelagic settling and/or low density turbidity currents	
LF18: Mass-flow breccia (sand-sized/>sand-sized)	Dark grey to black shale and silty shale; dolomitic; pyritic Medium to dark grey (rare black), matrix- or clast-supported grainstones, conglomerates, breccias; mono- or polymict; no fitting; tabular and equant clasts; sand to cobble-sized; well rounded to very angular carbonate clasts; minor up to granule-sized dolomitic siltstone clasts and sand-sized quartz grains; moderately to very poorly sorted; interstitial sulfides; background facies is LF13 and LF16	Very thinly to medium bedded, sometimes massive; mostly ungraded but sometimes fining- or coarsening upward	Deposition below storm wave base; hemipelagic settling and low-density turbidity currents Deposition from sediment gravity flows in slope environments; sand-sized subfacies from fine-grained turbidity currents and grainflows; > sand-sized subfacies from coarse-grained turbidity currents and debris flows	Barney Creek Fm Barney Creek Fm, Reward Dolostone
LF19: Rhythmite	Dark (rare medium) grey, very fine to fine dolarenite	Thickly laminated to thinly bedded; beds are massive or have an internal, mm-scale planar lamination with fining-upward; slump folds common; cm-scale growth faults; scouring	Deposition below storm wave base in slope environments; pelagic and hemipelagic fallout and deposition from dilute turbidity currents	Barney Creek Fm

on primary productivity in the surface ocean and the export production of organic matter. It can reach 3‰ in the modern ocean (Sarmiento and Gruber, 2006). Similar to the isotopic difference in the vertical water mass, a horizontal water mass difference can result from restriction, leading to more pronounced carbon isotopic excursions in platform carbonates compared to deep marine carbonates (Saltzman and Thomas, 2012). Further, supratidal sabkha environments can record extremely high carbon isotope ratios due to evaporation-induced fractionation (e.g., Stiller et al., 1985; Schmid, 2017). Other influences on the carbon isotopic composition of carbonate is mineralogical variation (< 1‰; Saltzman and Thomas, 2012), vital effects (negligible in the Precambrian), and secondary overprints. Such overprints can be evaluated by carbon-oxygen isotope relationships. Early diagenetic dolomitization has generally no effect on the carbon isotope composition of carbonate rocks (Hoefs, 2009 p. 203). For detailed reviews about carbon isotopes and their application to chemostratigraphy see Kump and Arthur (1999), Halverson (2013), and Saltzman and Thomas (2012).

In summary, as the carbon isotopic composition of carbonate rocks is influenced by several factors, its application in chemostratigraphy focuses on significant and systematic stratigraphic variability (> 1–2‰). Further, relative shifts are more important than actual values. Examples for successful carbon isotope chemostratigraphy in the Precambrian comes from numerous Neoproterozoic basins (e.g., Halverson et al., 2005; Hoffman et al., 2007; Macdonald et al., 2013; Smith et al., 2016) and led to reconstruction of a global carbon isotope curve for this time (e.g., Halverson et al., 2005, 2010; Cox et al., 2016). Low resolution carbon isotope records from the McArthur Group that did not show significant trends were previously reported by Lindsay and Brasier (2000). We produced high-resolution carbon isotope records from the studied drill cores to reevaluate whether the middle McArthur Group records systematic and significant variation in $\delta^{13}\text{C}_{\text{carb}}$ that can be used for chemostratigraphic correlation.

The carbon ($\delta^{13}\text{C}_{\text{carb}}$) and oxygen ($\delta^{18}\text{O}_{\text{carb}}$) isotope records from the middle McArthur Group were established by analyzing 485 samples. With the exception of 15 dolomitic siltstone samples (3%) from the HYC Pyritic Shale Member in Lamont Pass 3, all samples were carbonate lithofacies (i.e., inorganic carbon \gg organic carbon). Hand samples were cut perpendicular to lamination and carbonate powder was obtained by micro-drilling individual laminae or tight clusters. Macroscopic cements and secondary minerals (e.g., Coxco needles), or macroscopic siliciclastic and organic-rich components were avoided. Isotopic measurements were performed in dual inlet mode on a Nu Perspective isotope ratio mass spectrometer connected to a NuCarb carbonate preparation device in the Stable Isotope Laboratory at McGill University, Montréal, Canada. Approximately 80 μg of sample powder were weighed into glass vials and reacted individually with H_3PO_4 after heating to 90°C for one hour. The released CO_2 gas was purified cryogenically and isotope ratios were measured against an in-house reference gas. This method does not release CO_2 gas from ancient organic matter. Therefore, the result only reflects the isotopic composition of carbonate (inorganic) carbon. Samples were then calibrated to VPDB (Vienna Pee Dee Belemnite). Errors for both $\delta^{13}\text{C}_{\text{carb}}$ and $\delta^{18}\text{O}_{\text{carb}}$ were better than 0.05‰ (1 σ) based on repeated analyses of standards.

4. Facies analysis

We distinguish 19 lithofacies (LF) grouped into four facies associations (FA; Table 1; Figs. 3–7): supratidal to continental, shallow subtidal to intertidal, subtidal, and deep subtidal to slope. Genetically related lithofacies are grouped into facies associations that represent specific depositional environments with respect to sea level. Lithofacies grouped in the same facies association were likely deposited as lateral equivalents. We avoid terms such as ‘middle shelf’ in our facies nomenclature because this succession was deposited in a basin with complex architecture. Although carbonate rocks from the middle

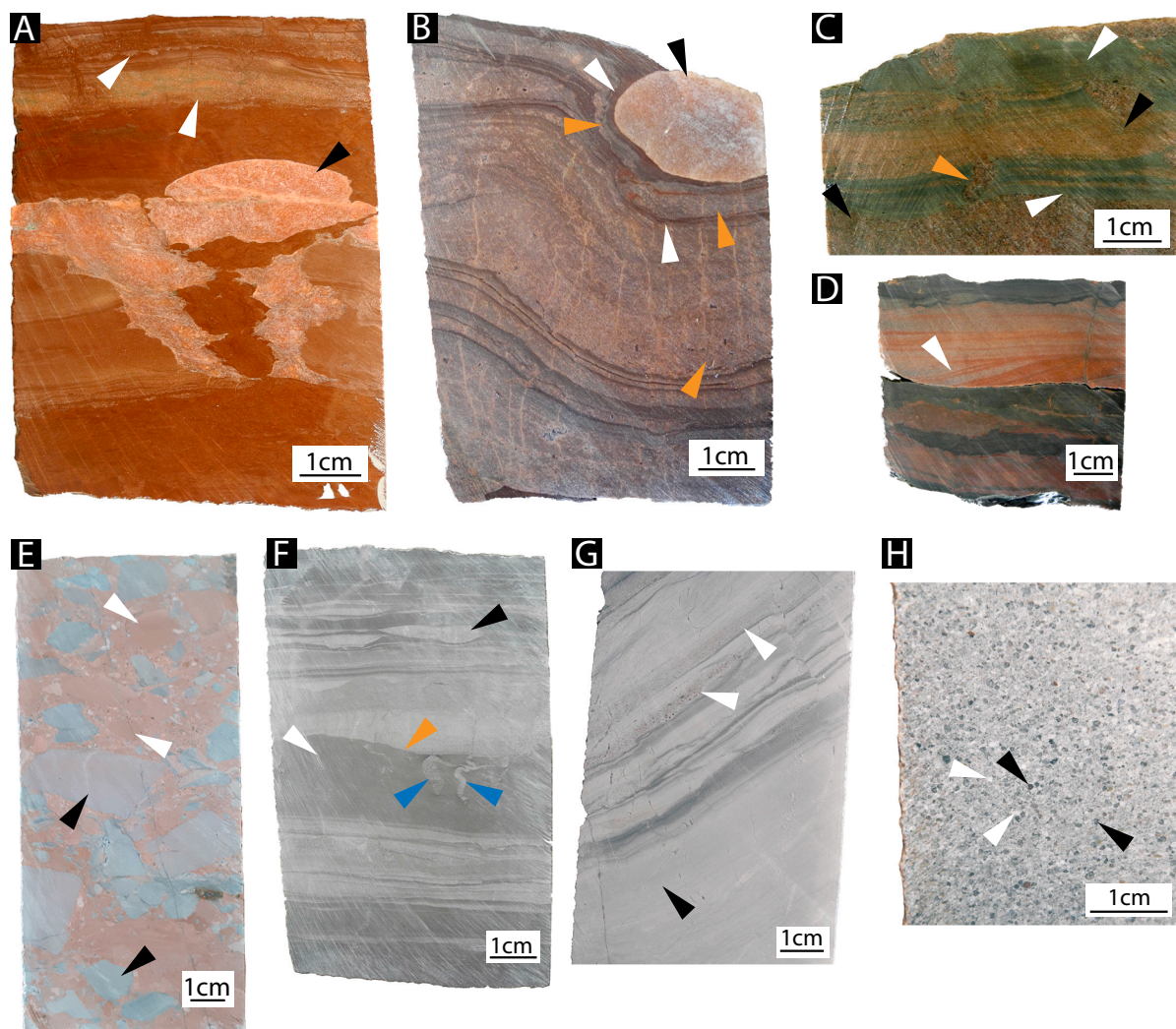


Fig. 3. Hand specimen photographs of various lithofacies from FA1 and FA2. A) Red siltstone (LF1) with cm-scale anhydrite nodule (black arrow). Note discontinuous laminae of sandstone (LF2; white arrows). Lamont Pass 3, 1060.3 m; Myrtle Shale. B) Anhydrite nodule (black arrow) displaces laminae of red siltstone (LF1; white arrows) and laminae and beds of sandstone (LF2; orange arrows). Lamont Pass 3, 1028.5 m; Myrtle Shale. C) Interbedding of green siltstone (LF1; white arrows) with sandstone (LF2; black arrows). Note mudcrack (orange arrow). Lamont Pass 3, 1041.5 m; Myrtle Shale. D) Cross-lamination (white arrow) in sandstone (LF2). Lamont Pass 3, 976.6 m; Myrtle Shale. E) Conglomerate (LF3) with carbonate (black arrows) and siltstone (white arrows) clasts. Lamont Pass 3, 861.5 m, Myrtle Shale. F) Interbedding of medium grey bedded dolarenite (LF4) with dark grey marine siltstone (LF6; white arrow). Dolarenite can occur as discontinuous lenses (black arrow). Note scour surface at base of dolarenite bed (orange arrow). The bedded dolarenite shows fining-upward immediately above the scour surface. Features pointed out by blue arrows are either deformed mudcracks or synaeresis cracks filled with dolarenite. Lamont Pass 3, 1144.9, Myrtle Shale. G) Dololite (LF8; black arrow) with two laminae of bedded dolarenite (LF4; white arrows) characterized by fining-upward and floating quartz (dark grains). Lamont Pass 3, 407.1 m; Lynott Formation. H) Marine sandstone (LF5) with quartz (black arrows) and carbonate grains (white arrows). Leila Yard 1, 252.1 m, Lynott Formation.

McArthur Group experienced recrystallization and the terms (dol)arenite and (dolo)lutite thus refer to crystal size instead of grain size, original grain size was presumably a major control on crystal size. Therefore, we treat crystal size as an approximation of initial grain size in these well preserved carbonate rocks.

4.1. FA1: supratidal to continental

4.1.1. LF1: red or green siltstone

This lithofacies is typical for the Myrtle Shale but also occurs in the Tooganinie Formation. It generally occurs in intervals that are a decimetre to a few metres thick. It consists of red or green siltstone (minor clay-rich siltstone or claystone, Fig. 3A, C), in places dolomitic. The rocks are laminated to massive and characterized by common anhydrite nodules (often displacing lamination; Fig. 3A, B) and anhydrite veins, occasional chicken wire texture, mudcracks (typically deformed), and flame and ball-and-pillow structures at interfaces with sandier facies.

Siltstones occasionally have starved ripples and a spotty texture with oxidation/reduction spots. The siltstones are typically finely laminated to finely bedded and may be locally truncated by sand channels (LF2, Fig. 3A, C, D) some of which contain intraclasts.

The common occurrence of mudcracks in red and green siltstone indicates frequent exposure. Interbedding of this lithofacies with various shallow marine facies suggests a marginal marine rather than a fully continental environment. In marginal marine environments, mudcracks are usually confined to upper intertidal to supratidal environments (e.g., Shinn, 1983b; Alsharhan and Kendall, 2003; James and Jones, 2016 p.159). A supratidal depositional environment is also consistent with the often observed displacive growth of anhydrite nodules because it indicates a diagenetic origin below the sediment surface, which is typical for supratidal sabkha environments (e.g., Evans et al., 1969; Kendall and Skipwith, 1969a,b; Butler, 1969; Warren and Kendall, 1985; Kirkham, 1997; Kendall and Alsharhan, 2011). However, the presence of nodular anhydrite does not necessarily prove

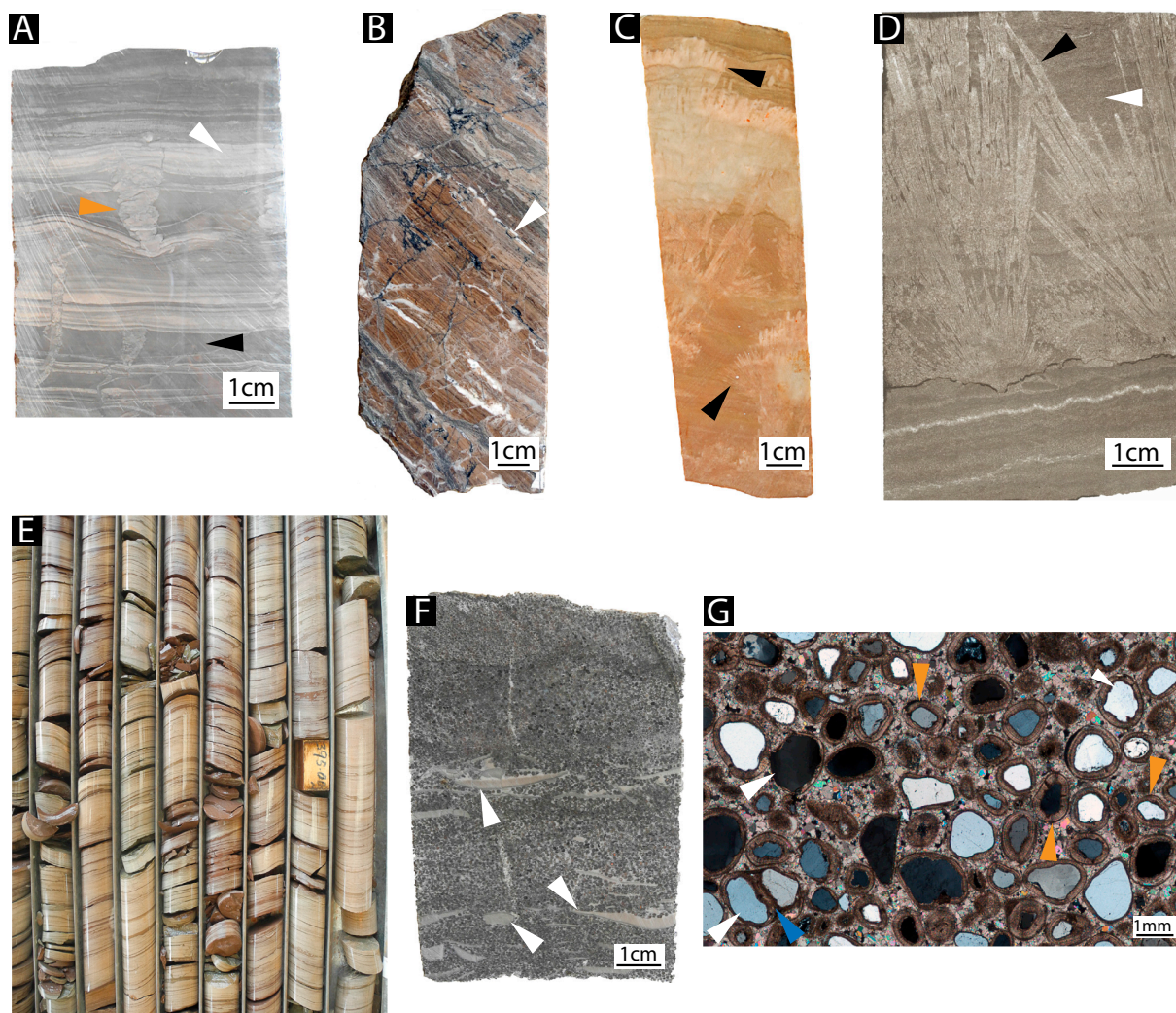


Fig. 4. Hand specimen, core tray, and thin section photographs of various lithofacies from FA2 and FA3. A) Marine siltstone (LF6, dark grey beds, black arrow) with bedded dolarenite (LF4, light grey laminae, white arrow) laminae. Note synaeris crack (orange arrow). Lamont Pass 3, 1174.6 m, Myrtle Shale. B) Silicified microbialaminite (LF7) with potential calcite-filled laminoid fenestrae (white arrow). Lamont Pass 3, 408.5; Lynott Formation. C) Pink-brown dololite (LF8) with acicular, radiating pseudomorphs (Coxco needles) interpreted by Winefield (2000) as former aragonite crystals. GRNT-79-3, 427.3 m; Coxco Member. D) Thin section photograph (transmitted light) of Coxco needles. Further magnification reveals that the matrix (white arrow) has an inequigranular, hypidiotopic, tightly packed mosaic fabric with dolomite crystals mostly ranging from 20 to 50 μm . The needles (black arrow) also have an inequigranular, hypidiotopic, tightly packed mosaic fabric but crystal sizes mostly range from 100 to 200 μm . GRNT-79-4, 217.0 m; Coxco Member. E) Interbedding of dolarenite with red and brown siltstone (LF9). Note cm-scale interbedding. Core diameter is 3.6 cm. GRNT-79-3, around 395.0 m. W-Fold Shale. F) Ooid grainstone (LF10) with intraclasts (white arrows). Lamont Pass 3, 1245.8 m; Myrtle Shale. G) Thin section photograph (cross-polarized light) of ooid grainstone (LF10). This rock has a packstone fabric with mostly 0.75–1.5 mm large, spherical to ellipsoidal, radial-fibrous ooids. Quartz grains form the nuclei (white arrows). Note the thin cortices (orange arrows) classifying most of these ooids as superficial (Flügel, 2004). Also note two aggregated ooids (blue arrow). The matrix has an inequigranular, xenotopic, tightly packed mosaic fabric. Lamont Pass 3, 1246.0 m; Myrtle Shale.

deposition in a sabkha environment because thick successions of laminated gypsum formed in subaqueous salina and shallow marine environments are transformed into nodular anhydrite during burial (Warren and Kendall, 1985). Nevertheless, considering that sulfate deposits formed in these environments are usually several meters thick (Warren and Kendall, 1985; Warren, 2010), we would expect to observe massive and nodular bedded anhydrite and not isolated anhydrite nodules that do not dominate the sediment by volume. Although both red and green siltstone contain mudcracks and anhydrite nodules, we interpret green siltstone to have formed more seaward where tides would have flooded the area more frequently and/or in ponds and creeks. In contrast, the red variety was likely deposited in higher supratidal environments, less frequently flooded by seawater and passing into a continental environment. This interpretation is consistent with red siltstone intervals being thicker and less frequently interbedded with

shallow marine facies (more common in Myrtle Shale; Fig. 8). The siliclastic composition demonstrates the vicinity of the supratidal environment to a continental source. Interbedding with sandstone (LF2) and conglomerate (LF3) causing flame and ball-and-pillow structures may be explained by episodic and rapid deposition following sheet flood events. In summary, the red and green siltstone lithofacies was deposited in upper intertidal to supratidal sabkha environments (Fig. 7) that were dominated by siliclastic deposition.

4.1.2. LF2: sandstone

The sandstone lithofacies (Fig. 3B, D) mostly occurs in the Leila Sandstone and Myrtle Shale. Individual beds are typically dm-scale in thickness but rarely reach a few meters. LF2 is typically a pink to grey/green quartz arenite to subarkose, which can be silty or dolomitic. The sandstone varies from very fine- to coarse-grained with subangular to

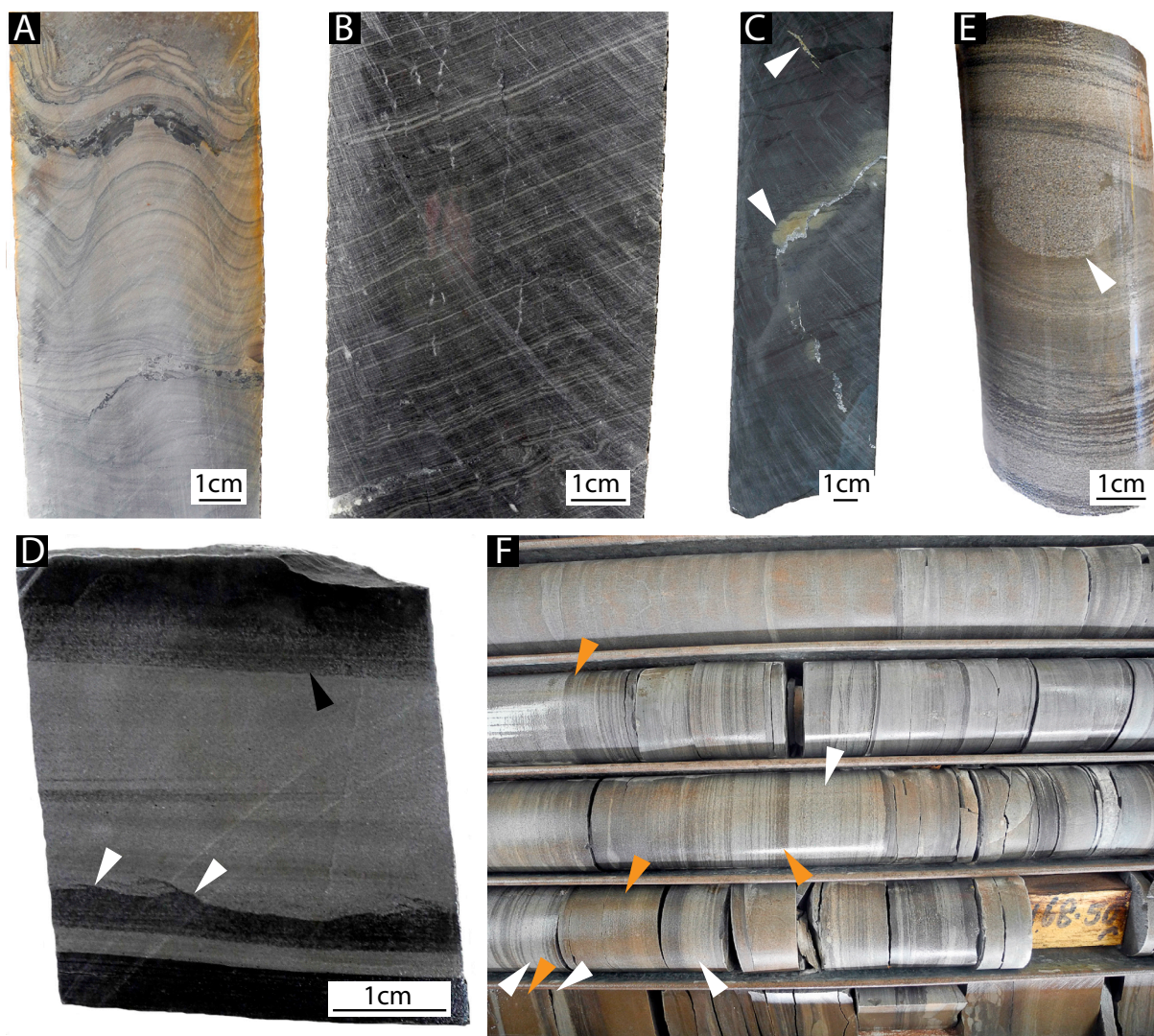


Fig. 5. Hand specimen and core tray photographs of various lithofacies from FA3 and FA4. A) Stromatolite (LF11) with ca. 2 cm synoptic relief. Lamont Pass 3, 932.2; Teena Dolostone. B) Muddy microbialaminite (LF12) with characteristic crinkly lamination. Lamont Pass 3, 624.9 m; Reward Dolostone. C) Dolomudstone (LF13) with pyrite (white arrows) along fractures. Lamont Pass 3, 711.8 m; Barney Creek Formation. D) Dolarenite bed (medium grey; LF14) in dolomitic siltstone (dark grey; LF16). Note loading at sharp base producing flame structures (white arrows) and gradual upper transition zone. GRNT-79-1, 22.3 m; Barney Creek Formation. E) Dolarenite (LF14) produced ball-and-pillow structure (white arrow) by sinking into dolomitic siltstone (LF16). Grain size appears larger as it is due to drill bit marks on outer side of core. GRNT-79-1, 206.2; Barney Creek Formation. F) Interbedded dolarenite (white arrows) with grey siltstone (orange arrows) facies (LF15). Note the regular interbedding of thin dolarenite laminae and beds. In contrast, dolarenite of LF14 is usually characterized by dm-scale beds. However, both were likely deposited by gravity-flows. Core diameter is 3.6 cm. GRNT-79-1, around 168.5 m; Barney Creek Formation.

well-rounded grains. LF2 is poorly to well sorted but always compositionally immature. Interbeds of LF1 and LF3 are common. The rocks are thickly laminated to thinly bedded, usually scour underlying beds, and often contain red and green siltstone intraclasts (LF1; subangular to rounded, tabular or circular). Fining-upward of laminae and beds, cross-lamination (Fig. 3D), anhydrite nodules/veins, and mudcracks (Fig. 3C) may occur.

Episodic floods (probably sheet floods) likely supplied coarser-grained material to silt-dominated supratidal sabkha environments (and possibly also peritidal environments; Fig. 7). These episodic events ripped-up LF1 intraclasts. Subsequent drying explains the observed mudcracks and anhydrite nodules.

4.1.3. LF3: conglomerate

Conglomerates (Fig. 3E) are rare but occur in the Myrtle Shale and W-Fold Shale. They usually occur in cm- to dm-thick intervals but occasionally reach several meters. They can be thinly bedded but

dominantly comprise a single massive bed with an erosional base. The conglomerates are polymictic, grey to brown, and are composed of granule- to boulder-sized clasts of siltstone (LF1), sandstone (LF2), and occasionally dolostone (intertidal facies, Fig. 3E). The conglomerate is clast-supported, and clasts are sub-rounded to very well-rounded. Silicification and interbeds of green or red siltstone (LF1) can occur.

Close association of this lithofacies with red and green siltstone (LF1) and sandstone (LF2) suggests deposition in supratidal sabkha environments, comparable to the depositional environments inferred for LF2 (Fig. 7). However, occurrence of occasional dolostone clasts (LF4) indicates reworking of intertidal environments. This suggests that some conglomerates were also deposited in intertidal settings.

4.2. FA2: shallow subtidal to intertidal

4.2.1. LF4: bedded dolarenite

This lithofacies (Fig. 3F) occurs in all investigated stratigraphic

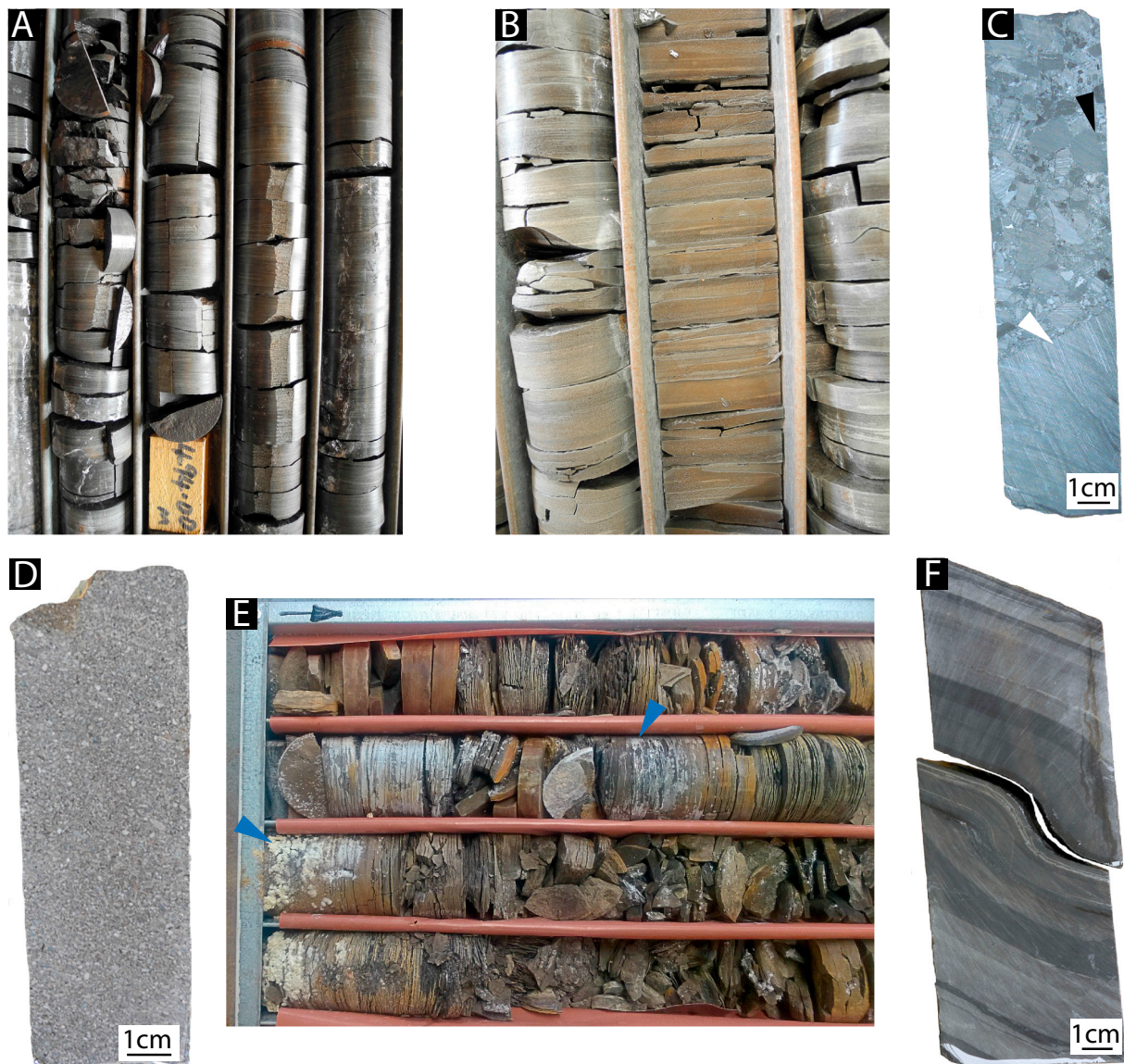


Fig. 6. Hand specimen and core tray photographs of various lithofacies from FA4. A) Dolomitic siltstone (LF16) is the most common facies in the Barney Creek Formation. Core diameter is 3.6 cm. GRNT-79-8, around 494.0 m; Barney Creek Formation. B) Note typical thick lamination in dolomitic siltstone (LF16). Core diameter is 3.6 cm. GRNT-79-1, 259.8 m; Barney Creek Formation. C) Clast-supported, poorly sorted, and ungraded mass-flow breccia (LF18; > sand-sized subfacies) with subangular to subrounded clasts of muddy microbialaminite (white arrow) and dolomudstone (black arrow). Core diameter is 3.6 cm. MANT-79-2, 295.0 m; Barney Creek Formation. D) Clast-supported mass-flow breccia (LF18, sand-sized subfacies). This subfacies has a similar origin and composition to dolarenite (LF14, compare to D and E). However, this subfacies of mass-flow breccia is typically polymict and coarser grained. GRNT-79-7, 121.0 m; Barney Creek Formation. E) Strongly weathered, pyritic black shale (LF17). White crust (blue arrows) is sulfate formed by pyrite weathering. Note fine lamination of this lithofacies. Core diameter is 3.6 cm. GR10, around 60.0 m; Barney Creek Formation. F) Rhythmite (LF19) with slump fold. Typical for this lithofacies is the ‘rhythmic’ alternation of lighter grey and darker grey dolarenite and dololutite. Lamont Pass 3, 758.3 m; Barney Creek Formation.

units. Bedded dolarenite intervals are typically 10s of centimeters to several meters thick and interbedded with lithofacies from FA1, FA2, and dolomudstone (LF13) from FA3. This lithofacies is typically light to medium grey (rare dark grey), and can be silicified or contains floating quartz (Fig. 3G). In intervals where floating quartz is common, laminae and thin beds of marine sandstone (LF5) and marine siltstone (LF6) are common. The grain size ranges from dolosiltite to dolorudite (mostly dolosiltite and very fine dolarenite). Pyrite and organic matter streaks are common when bedded dolarenite is interbedded with dolomudstone (LF13). Furthermore, pyrite and base metals sulfides can occur in brecciated intervals. This lithofacies is generally thickly laminated to medium bedded; however, some intervals are massive. Parallel-planar lamination dominates but nodular bedding, carbonate nodules, wavy and/or discontinuous shale and siltstone laminae, or cross-lamination

may occur. Furthermore, laminae, beds, and channels of the same lithofacies or marine sandstone (LF5) with (low-angle) cross-lamination are common. Individual beds or bed sets can fine-upwards. This lithofacies can host cm- to dm-thick, brecciated and silicified horizons interpreted to represent exposure surfaces. Sedimentary structures include scour surfaces (Fig. 3F), rare silicified or calcite-filled fenestrae (laminoid or irregular, 1–2 mm high, up to 10 mm long), rip-up clasts and mud chips, discrete intraclast beds (tempestites?), and soft-sediment deformation such as loading and ball-and-pillow structures. Acicular and radiating pseudomorphs (Coxco needles) several centimeters across, interpreted by Winefield (2000) as aragonite pseudomorphs, are rare and confined to the Coxco Member. Sand-filled mudcracks and anhydrite veins may occur when interbedded with FA1, and molar tooth structures are common in darker varieties when this facies is

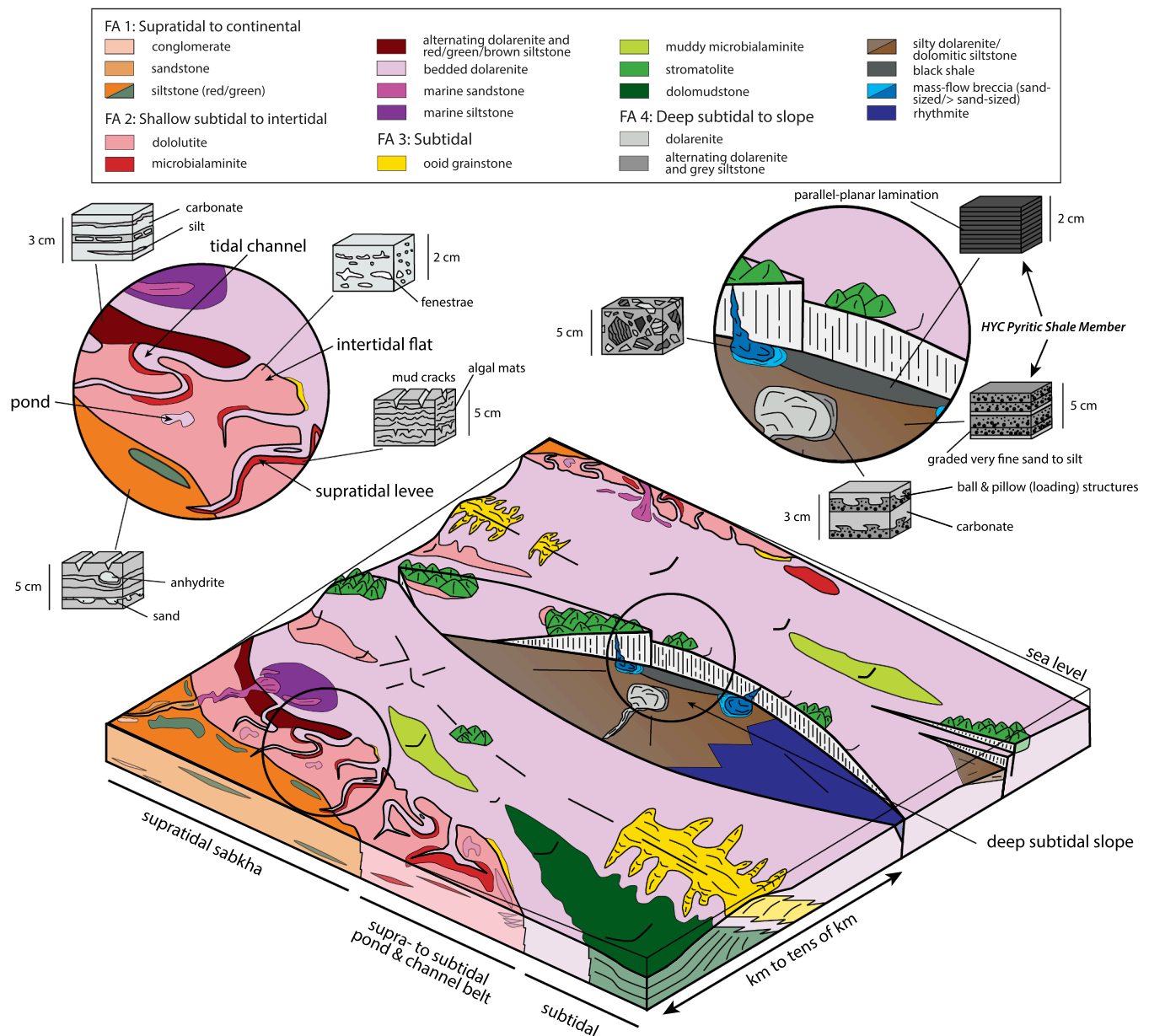


Fig. 7. Schematic block diagram depicting interpreted depositional environments, including sub-basin and paleohigh settings, of middle McArthur Group (Tooganinie Formation to Hot Spring Member of Lynott Formation; Fig. 2). Insets are enlargements of depositional settings and grey-scale block figures show sedimentary structures as observed in drill core. Very shallow seafloor inclination would have permitted peritidal environments to migrate hundreds of kilometers with relative sea level fluctuations of meters to a few tens of meters.

interbedded with muddy microbialaminite (LF12 of FA3).

Facies relationships (interbedding with other lithofacies from FA2, occasional interbedding with FA1 and FA3), stratigraphic position in shoaling-upward parasequences, and sedimentary structures (e.g., mudcracks, fenestrae) indicate that this lithofacies represents deposition in shallow subtidal to upper intertidal, and occasionally even supratidal environments. However, the supratidal environments in which bedded dolarenite may have occasionally been deposited (e.g., beach ridges and tidal channel levees) were likely seaward of the sabkha and supratidal belt of FA1 and generally smaller scale and more frequently flooded (cf. Shinn et al., 1969; Maloof and Grotzinger, 2012). Comparison with modern equivalent depositional environments such as the Bahamas (e.g., Field, 1931; Illing, 1954; Shinn et al., 1969, 1983b; Rankey, 2002; Rankey and Morgan, 2002; Reijmer et al., 2009; Maloof and Grotzinger, 2012) and the Trucial Coast along the Persian Gulf (e.g., Kendall and Skipwith, 1969a,b; Wagner and van der Togt, 1973;

Alsharhan and Kendall, 2003; Kendall and Alsharhan, 2011) suggests that bedded dolarenites from the middle McArthur Group were likely deposited in a complex mosaic of environments (Fig. 7) including shallow subtidal shoals, lagoons, shoreface, beaches, beach ridges, tidal channels, levee crests, and tidal channel bars. Therefore, this lithofacies lumps carbonate rocks from different subenvironments (cf. Kunzmann et al., 2014) that are difficult to distinguish even in modern settings (e.g., sediments in ponds, tidal channels, and adjacent marine areas; Shinn et al., 1969, 1983b). Further complication arises from the poorly understood preservation potential of modern subenvironments such as tidal channels and ponds (Wright, 1984; Maloof and Grotzinger, 2012), and differences between modern and Proterozoic environments such as the lack of bioturbation. Nevertheless, the presence of sedimentary structures allows evaluating depositional processes in more detail on the scale of individual beds. For example, bedded dolarenite beds with cross-lamination and/or mudcracks are comparable to modern

supratidal beach ridge deposits (Maloof and Grotzinger, 2012) and intertidal channel bar and supratidal levee sediments (Shinn et al., 1969, 1983b). Small cm-scale channels with internal cross-lamination are similar to storm deposits in shallow subtidal shoreface environments (Inden and Moore, 1983) and beaches, tidal channels, and intertidal flats (e.g., Kendall and Skipwith, 1969b; Shinn et al., 1969, 1983b; Kendall and Alsharhan, 2011). Scour surfaces, rip-up clasts and mud chips, and intraclast beds were likely formed by storms and strong tidal currents in shallow subtidal subenvironments like lagoons, shoreface, and tidal channels (Kendall and Skipwith, 1969b; Shinn, 1983b), and supratidal beach ridges (Shinn et al., 1969). Although fenestrae-like voids can form in subtidal grainstones (Shinn, 1983a), real fenestrae most commonly occur in upper intertidal to supratidal environments (Shinn, 1968, 1983b,a; Flügel, 2004) such as tidal channel levees (Shinn, 1983b). Their scarcity in rocks from the middle McArthur Group might be due to compaction, which has been shown to obliterate these features if early cementation did not occur (Shinn and Robbin, 1983).

The occasional occurrence of floating quartz and the continuum with marine sandstone (LF5) indicate proximity to a terrigenous source. The occurrence of molar tooth structures in darker, presumably more organic-rich, varieties when interbedded with muddy microbialaminite (LF12; FA3) can be explained by diagenetic remineralization of organic matter (e.g., Hodgskiss et al., 2018). Ball-and-pillow structures and other loading-related soft sediment deformation suggest rapid sedimentation.

4.2.2. LF5: marine sandstone

Marine sandstone (Fig. 3H) occurs in the Myrtle Shale and particularly in the Hot Spring Member of the Lynott Formation. It typically occurs as centimeter to decimeter thick intervals and is associated with FA1 and other lithofacies of FA2, in particular bedded dolarenite (LF4). This lithofacies is a light to medium grey (rare dark grey) quartz arenite, medium to coarse grained, rounded to well rounded, and well sorted. It often contains well rounded carbonate grains (Fig. 3H) and a carbonate matrix (sometimes silicified). Marine sandstone often contains interbeds of bedded dolarenite with floating quartz and generally represents a continuum with bedded dolarenite. Pyrite, disseminated or concentrated in spots several mm in diameter, occurs in places. This lithofacies is usually massive but often contains tabular, mm- to cm-large rip-up clasts of bedded dolarenite, siltstone, or shale.

The common carbonate matrix, the compositional continuum and interbedding with bedded dolarenite (LF4) with floating quartz, and interbedding other facies from FA2 and FA1 suggests that marine sandstone was also deposited in shallow subtidal to intertidal environments (Fig. 7). Roundness and sorting suggest significant transport from the terrigenous source to the site of deposition, unless the quartz grains were sourced from coastal outcrops of older siliciclastic units, as reported from Holocene sediments along the Trucial Coast (Kendall and Skipwith, 1969b; Kendall and Alsharhan, 2011). Further considering similar deposits along the Trucial Coast, varying proportions of carbonate (grains and matrix) and quartz can be explained with a shift in depositional environment from beaches and intertidal flats, which in some areas of the Trucial Coast are entirely composed of quartz grains, to environments more seawards (Kendall and Skipwith, 1969b; Kendall and Alsharhan, 2011). Rip-up clasts suggest occasional storm events or strong tidal currents.

4.2.3. LF6: marine siltstone

The marine siltstone lithofacies (Figs. 3F and 4A) usually occurs as decimeter-thick intervals in the Tooganinie Formation. It is typically interbedded with FA1 and FA2. Marine siltstone is dark grey/green to black and often dolomitic. It is generally thickly laminated with planar-parallel or wavy lamination. It can have discontinuous or continuous laminae, beds, or channels of LF4 with uni- or bidirectional cross-lamination. Starved ripples, mudcracks, syneresis cracks (Fig. 4A) and

ball-and-pillow structures may occur.

Interbedding with FA1 and FA2 suggests deposition in shallow subtidal to intertidal environments (Fig. 7). This interpretation is supported by the occasional occurrence of mudcracks. This lithofacies was likely deposited in subenvironments with less hydrodynamic energy than LF5. However, the occasional presence of channels filled with LF4 as well as starved ripples indicate periods of higher energy, likely related to storms and/or strong tidal currents. Bi-directional cross-lamination likely indicates tidal influence. Ball-and-pillow structures again suggest rapid deposition.

4.2.4. LF7: microbialaminite

Decimeter thick intervals of microbialaminite (Fig. 4B) occur in all stratigraphic units. This lithofacies is usually interbedded with all other facies of FA2 or overlies stromatolites (LF11) of FA3 in shoaling upward cycles. Rocks of this lithofacies are composed of light to medium grey (rare dark grey) doloboundstone, which is often silicified (Fig. 4B). Microbialaminite is characterized by an alternation of about 1 mm thick dark grey, flat, crinkly, and undulating laminae, which we interpret as microbial, with about 1–3 mm thick light to medium grey dolomite laminae. Microscopy demonstrates that this lithofacies contains up to 30% subangular to subrounded, up to silt-sized, quartz grains, equally distributed between the laminae. Irregular domal structures with ca. 5 mm synoptic relief can also occur. Fenestrae (silicified or calcite-filled, laminoid or irregular, 1–2 mm high and up to 10 mm long), tepees, and mudcracks can occur. This facies can be vuggy or brecciated and discrete beds of intraclast breccias may be present.

Microbial mats comparable to microbialaminite from the McArthur Group occur in modern intertidal to lower supratidal flat environments such as Shark Bay, Western Australia (e.g., Logan, 1961; Logan et al., 1964; Hoffman, 1976; Playford et al., 2013; Suosaari et al., 2016), the Arabian Gulf (e.g., Kendall and Skipwith, 1968; Kendall and Skipwith, 1969a; Kinsman and Park, 1976; Duane and Al-Zamel, 1999; Alsharhan and Kendall, 2003; Kendall and Alsharhan, 2011), and the Bahamas (e.g., Shinn et al., 1969; Rankey and Morgan, 2002; Maloof and Grotzinger, 2012). Deposition of LF7 in inter- to lower supratidal environments is supported by the occurrence of mudcracks, fenestrae, and peritidal tepees (Shinn, 1968, 1983a,b; Kendall and Warren, 1987; Alsharhan and Kendall, 2003). Along the arid Trucial Coast of the Arabian Gulf, different algal mat types can be distinguished based on morphology. These mat types occur in distinctive geographical zones parallel to the shoreline, which are controlled by the frequency of wetting (Kendall and Skipwith, 1968; Kendall and Skipwith, 1969a; Kinsman and Park, 1976; Alsharhan and Kendall, 2003; Kendall and Alsharhan, 2011). On Andros Island in the Bahamas, algal mats occur in different microenvironments such as levee crests and intertidal flats protected by levees (Maloof and Grotzinger, 2012). However, a distinction between different mat types and microenvironments in microbialaminite from the McArthur Group is not possible due to varying preservation potential (Park, 1977), the effects of burial and compaction on mat morphology, and lack of exposure. Nevertheless, continuous algal mats only occur in protected environments where wave and tidal scour is weak (Hoffman, 1976). In conclusion, this lithofacies was likely deposited in protected inter- to lower supratidal environments (Fig. 7). Due to lack of grazing pressure in the Precambrian, this lithofacies may have also been deposited in low-energy shallow subtidal environments.

4.2.5. LF8: dololite

Dololite occurs in all stratigraphic units and typically appears as decimeter to rarely meter thick intervals. It is generally interbedded with FA2 or stromatolite (LF11) of FA3. This lithofacies is thinly laminated to massive and consists of light grey to pink, rarely dark grey dololite/micrite (Figs. 3G and 4C). Silicified fenestrae are common (laminoid or irregular, 1–2 mm high and up to 10 mm long) and acicular, radiating, mm- to cm-scale pseudomorphs (Fig. 4C, D; Coxco

needles), interpreted by Winefield (2000) as aragonite pseudomorphs, often occur in pink dololite of the Coxco Member. Irregular, cm-scale, partly brecciated silicified intervals, which we interpret as karst surfaces, can occur. Mudcracks filled with bedded dolarenite (LF4), channels and continuous or discontinuous laminae (scoured bases) of LF4 with starved ripples, cross-lamination, or fining-upward grading may occur.

Similar to bedded dolarenite (LF4), stratigraphic position in shallowing upward parasequences and sedimentary structures suggest that this lithofacies was likely deposited in various shallow subtidal to upper intertidal, and occasionally supratidal environments. Considering the crystal size as indicator for original grain size, comparison with modern carbonate environments such as Bahamas (e.g., Shinn et al., 1969, 1983b; Reijmer et al., 2009; Maloof and Grotzinger, 2012) and the Trucial Coast along the Arabian Gulf (e.g., Kendall and Skipwith, 1969b; Alsharhan and Kendall, 2003; Kendall and Alsharhan, 2011) suggests that dololites from the McArthur Group were likely deposited in various depositional environments such as protected inner lagoons/platforms; the lee side of banks, shoals, stromatolite build ups; on levee crests; in intertidal ponds and low-energy parts of tidal channels. Similar to the bedded dolarenite (LF4), the dololite lithofacies encompasses multiple potential depositional environments (Fig. 7). However, depending on sedimentary structures present, a more detailed interpretation may be possible for individual beds and bed sets. For example, intervals with karst surfaces, mudcracks, and fenestrae were deposited in upper inter- to supratidal environments such as ponds, levee crests, and flats. Beds with channels filled with LF4 and internal cross-lamination and starved ripples, as well as intraclasts beds, were likely deposited during storms or strong tidal activity.

4.2.6. LF9: interbedded dolarenite with red, green, or brown siltstone laminae

This lithofacies typically occurs as decimeter to meter thick intervals in the W-Fold Shale, interbedded with other facies from FA2. LF9 is composed of alternating cm-scale, light grey to pink dololite, dolosiltite, or dolarenite intervals with up to 1 cm-thick, red, green, or brown siltstone or shale laminae (Fig. 4E). This facies is typically very thinly bedded and the siliciclastic laminae and beds are wavy and continuous or discontinuous. Intraclasts, mud chips, flame structures, scour surfaces, and acicular, radiating aragonite pseudomorphs may occur.

Intimate association of this lithofacies with other facies from FA2 suggest deposition in shallow subtidal to intertidal environments. The siltstone laminae are very similar to LF1, further supporting a peritidal origin, and indicate a frequent variation between carbonate-dominated and siliciclastic-dominated deposition. The siltstone laminae may have been deposited in intertidal ponds close to a fluvial source. Lack of mudcracks suggest deposition seawards of upper intertidal environments. Intraclasts and mud chips indicate frequent storm and/or strong tidal energy. Flame structures suggest rapid deposition. In summary, we envision deposition as facies mosaic that ranged from shallow subtidal (carbonate-dominated laminae; subenvironments comparable to bedded dolarenite (LF4) and dololite (LF8)) to lower intertidal environments in the vicinity to a terrigenous source such as a fluvial system/estuary (Fig. 7).

4.3. FA3: subtidal

4.3.1. LF10: ooid grainstone

Ooid grainstone is a lithofacies in the Tooganinie Formation and occurs as dm-thick intervals. It is interbedded with FA3, FA2, and FA1. This lithofacies is composed of medium grey dolopackstone and dolograins with mostly 0.75–1.5 mm large ooids (Fig. 4F, G). The ooids are mostly symmetrical, and spherical to ellipsoidal, with the shape being controlled by large nuclei composed of quartz grains (Fig. 4G). Most grains are superficial ooids, with the cortex being less than half as

thick as the nucleus (Fig. 4G; Flügel, 2004). The ooids are mostly radial-fibrous, although this might be a secondary diagenetic feature as the radially oriented crystals transect individual laminae. Aggregation of several ooids can occur (Fig. 4G). Ooid grainstones are massive and often silicified. Rip-up clasts of bedded dolarenite (LF4) and dololite (LF8) occur (Fig. 4F).

Ooids require environments with agitated water (e.g., Bathurst, 1975), and oolitic sands forming linear or parabolic bars occur in the Bahamas (e.g., Hine, 1977; Halley et al., 1983; Rankey et al., 2006; Reeder and Rankey, 2008; Rankey and Reeder, 2011), Shark Bay, Western Australia (e.g., Jahnert and Collins, 2011; Playford et al., 2013), and the Arabian Gulf (Kendall and Skipwith, 1969b; Kendall and Alsharhan, 2011). Ooid shoals commonly form in shallow subtidal environments by strong tidal currents at platform margins, in straits and seaways between (barrier) islands (e.g., Rankey et al., 2006; Reeder and Rankey, 2008; Rankey and Reeder, 2011; James and Jones, 2016 p. 167), in subtidal hypersaline lagoons (e.g., Jahnert and Collins, 2011; Playford et al., 2013), or in subtidal platform interiors where wave and storm action are more important than tides (James and Jones, 2016 p. 174). We generally interpret ooid grainstones to reflect high-energy shallow subtidal environments (Fig. 7). However, Inden and Moore (1983) point out that many thin ooid grain- and packstone beds were likely deposited in beach environments which can be identified by interbedding with supratidal facies. This association is seen in the Tooganinie Formation. Therefore, it is possible that the ooid grainstones we observe in the Tooganinie Formation were also deposited in beach environments (Fig. 7).

4.3.2. LF11: stromatolite

Stromatolites occur in all stratigraphic units and are typically decimeter to a few meters thick. They are typically interbedded with other facies from FA3, and also facies from FA1 and FA2. Stromatolites are composed of medium grey (rare black) doloboundstone (Fig. 5A). They can be silicified and entirely brecciated, or may grow on brecciated surfaces and may be brecciated at the top. Laterally linked domal and columnar forms dominate and reach a few dm in height. *Conophyton* can also occur. The synoptic relief typically does not exceed 10 cm. However, due to limited exposure in drill cores, the macroscale geometry of stromatolites (e.g., dm- to m-scale synoptic relief) and their occurrence as bioherms versus biostromes is difficult to assess. Areas between domes are typically filled by micrite.

We interpret stromatolites from the middle McArthur Group to have been deposited dominantly in shallow subtidal environments (Fig. 7), and possibly more rarely in intertidal settings. This interpretation is consistent with lack of sedimentary structures indicating exposure. Furthermore, high-relief stromatolites comparable to those from the McArthur Group are known from modern subtidal environments such as Shark Bay, Western Australia (e.g., Logan, 1961; Logan et al., 1964; Hoffman, 1976; Reid et al., 2003; Jahnert and Collins, 2011; Jahnert and Collins, 2012; Playford et al., 2013; Suosaari et al., 2016) and the Bahamas (Dravis, 1983; Dill et al., 1986). High-relief stromatolites are typical in areas with high wave and tidal energy, such as headlands (e.g., Hoffman, 1976). Common brecciation of stromatolites may indicate deposition as part of barrier complexes subjected to storms.

4.3.3. LF12: muddy microbialaminite

Muddy microbialaminite occurs in dm-thick intervals in the Reward Dolostone and Lynott Formation. It is usually interbedded with lithofacies of FA2 and FA3. This lithofacies is composed of dark grey to black (presumably organic matter-rich) doloboundstone (Fig. 5B). It can be clay-rich and is rarely silicified. Interbeds of dolomudstone (LF13) can occur. Fine-grained pyrite may occur along laminae. This lithofacies is characterized by an alternation of ca. 1 mm thick flat, crinkly, or undulating laminae (sometimes disrupted or buckled up), which we interpret as microbial, with about 1–3 mm thick, grey dolomite laminae. Molar tooth structures are common but fenestrae (laminoid, calcite-

filled, 1 mm high and 5–10 mm long) are rare.

In Hamelin Pool of Shark Bay, Western Australia, high-relief stromatolites comparable to LF11 occur in subtidal settings at headlands characterized by intense tidal and wave activity, and the steepest slope along this coastline. In contrast, more protected peritidal areas of the coastline, such as bights and embayments have shallower slopes and have significantly lower wave and tidal activity (Hoffman, 1976). These areas are not dominated by high-relief stromatolites but instead colonized by microbial mats (Jahnert and Collins, 2012) comparable to microbialaminite and muddy microbialaminite from the McArthur Group. The hypersaline conditions prevent grazing stress at Hamelin Pool, but lack of predators in the Precambrian would suggest that microbial mats may have been common in Proterozoic low-energy shallow subtidal environments. In contrast to microbialaminite (LF7), we interpret these dark grey to black ('muddy') microbialaminites to have been generally deposited in mostly quiet submerged environments (Fig. 7), such as lagoons, to account for their high clay and presumably high organic-matter content.

4.3.4. LF13: dolomudstone

Dolomudstone occurs as decimeter- to meter-thick intervals interbedded with lithofacies of FA2 and FA3 in the Barney Creek Formation, Reward Dolostone, and the Lynott Formation. This lithofacies is generally composed of dark grey to black, homogeneous dololite or dolosiltite (Fig. 5C). The rocks are clay- and presumably organic matter-rich, and may also be silty. Interbeds of muddy microbialaminite (LF12) or black shale (LF17) can occur, and it can be transitional with dololite (LF8). Pyrite and base metals sulfides may occur in streaks, spots, along fractures (Fig. 5C), disseminated or stratiform. This lithofacies is thinly laminated to massive, may have nodular bedding or contain pale grey nodules (sometimes plastically deformed). Slumping, loading and ball-and-pillow structures may occur, as well as molar tooth structures. Subhorizontal organic matter flakes and rip-up clasts of dolarenite may occur. Discontinuous or wavy shale laminae and dolarenite laminae with cross-lamination or starved ripples can also occur. This facies can contain subhorizontal flakes of organic matter that are up to several mm in length. Some intervals occur as 'flake breccia', which is matrix supported, and has pale grey dolostone clasts that are subangular to rounded, mostly tabular, and subhorizontal.

We interpret this lithofacies to have been deposited in quiet subtidal environments (Fig. 7). This is consistent with the interbedding with facies from FA2 and FA3 and the transitional character with dololite (LF8). Deposition above wave base is indicated by the occurrence of rip-up clasts, and cross-lamination and starved ripples in dolarenite laminae. The flake breccia intervals may have also been formed by storm events. Beds showing loading and ball-and-pillow structures were rapidly deposited, and beds with slumping suggest deposition on an inclined sea floor. This lithofacies likely represents deposition in a similar environment as the muddy microbialaminite (LF12). The absence of microbial laminae may be due to higher sedimentation rates or greater water depth, both factors that would inhibit photosynthetic microbial communities.

4.4. Deep subtidal to slope

4.4.1. LF14: dolarenite

This lithofacies generally occurs as decimeter- to a few meter-thick intervals in the undifferentiated Barney Creek Formation. It is often interbedded with LF15, LF16, and LF18. The dolarenite lithofacies is composed of medium grey, dolosiltite to dolarenite (Fig. 5D), with very fine- to fine-grained dolarenite clearly dominating. This facies can be silty or contain rounded quartz grains. It can also contain pyrite, either disseminated or as spotty accumulations. This lithofacies is thinly laminated to medium bedded and rarely has (low-angle) cross-lamination, starved ripples, or HCS. Beds are either not graded or show fining- or coarsening upward. Bed bases are often sharp and scour underlying

beds (Fig. 5D). However, tops are often transitional with overlying lithofacies (Fig. 4D). Loading and ball-and-pillow structures sinking into underlying dolomitic siltstone (LF16) beds are common (Fig. 5E), and slumping may also occur. Dolarenite can have mm to cm scale, rounded, intraclasts of LF4, LF11, and LF16. Common are sub-mm to mm scale organic matter flakes, which are either disseminated, concentrated in certain beds, or form discontinuous laminae.

It is likely that this lithofacies represents a range of different depositional environments. However, the mostly decimeter-scale thickness, scoured bases, sand-dominated grain- and packstone textures, occasional low-angle cross-lamination, grading, organic matter flakes, and interbedding with hemipelagic facies (LF16) suggest deposition from sediment gravity flows (Fig. 7) such as grainflows and turbidity currents in deep subtidal slope environments (Coniglio and Dix, 1992; James and Jones, 2016 p. 216). The material was sourced from platform margin environments such as shoals. Another possible origin of certain beds is deposition by storms near storm wave base. This interpretation is consistent with the occurrence of HCS and scoured bases. However, the common interbedding with LF16 generally favors deposition from gravity flows.

4.4.2. LF15: interbedded dolarenite with grey siltstone

This is a common lithofacies in the undifferentiated Barney Creek Formation that occurs as decimeter- to meter-thick intervals. It is typically interbedded with silty dolarenite/dolomitic siltstone (LF16). Interbedding of medium grey dolosiltite and dolarenite (occasionally with floating quartz) with dark grey dolomitic siltstone characterizes this lithofacies (Fig. 5F). The alternation is mostly on a cm-scale; however, it can reach 10–20 cm in thickness. This lithofacies is thickly laminated to very thinly bedded. Dolarenite laminae and beds typically scour underlying siltstone laminae/beds. They commonly display loading, flame, and ball-and-pillow structures and may internally show cross-lamination, SCS, and starved ripples. They can also have mud chips and organic matter flakes. Slumping, cm-scale growth faults, and carbonate nodules occasionally occur.

We interpret the depositional environment of this lithofacies to be comparable to that of dolarenite (LF14): deposition mostly from sediment gravity flows (Fig. 7). However, LF15 is marked by much thinner (mostly cm-scale) but regularly occurring, gravity flow deposits (dolarenite), interbedded with dolomitic siltstone (LF16) as background sediment.

4.4.3. LF16: silty dolarenite/dolomitic siltstone

This lithofacies (Fig. 6A, B) occurs as decimeter- to tens of meters-thick intervals in the HYC Pyritic Shale Member, overlying undifferentiated Barney Creek Formation, and Caranbirini Member of the Lynott Formation. It is by far the most common lithofacies of the Barney Creek Formation in sub-basins. Interbedding with other lithofacies of FA4 is typical. Lithofacies 16 represents a continuum between medium to dark grey silty dolostone and dark grey to black dolomitic siltstone and very fine sandstone, which have been distinguished in logs. The compositional difference is typically also manifested in bedding differences. Whereas the silty dolarenite subfacies is very thinly to thinly bedded, the dolomitic siltstone subfacies is thickly laminated (Fig. 6B). In the HYC Pyritic Shale Member, the dolomitic siltstone is generally pyritic and bituminous. These rocks generally have a parallel-planar and occasionally wavy lamination. Individual laminae and beds may be normally graded. Carbonate nodules, slumping, growth faults, loading (where in contact with the dolarenite facies) and rare dolarenite clasts may occur. Silty dolarenite has rare HCS, low-angle cross-lamination (tangential or straight foresets), and starved ripples.

The dolomitic siltstone sub-facies was likely deposited below storm wave base as indicated by absence of wave- or storm-induced sedimentary structures. However, deposition in slightly shallower environments, around storm wave base, of the silty dolarenite sub-facies is suggested by occasional HCS, low-angle cross-lamination and starved

ripples. This is consistent with the higher abundance of carbonate, which is generally produced in shallow subtidal environments and subsequently supplied to shallower and deeper depositional environments by storm-generated currents. Both sub-facies were likely deposited as a result of hemipelagic settling and/or low-density turbidity currents (Fig. 7; Wignall, 1994). Bull (1998) similarly suggested sub-wave-base environments for fine-grained siliciclastic sediments of the Barney Creek Formation.

4.4.4. LF17: black shale

Black shale occurs as decimeter- to meter-thick intervals in the HYC Pyritic Shale Member and the undifferentiated Barney Creek Formation. It is interbedded with dolomitic siltstone of LF16. This lithofacies is composed of dark grey to black shale and silty shale (Fig. 6E). It is typically pyritic and can also be dolomitic. Black shales are parallel-planar laminated and fissile or rubbly.

Deposition below storm wave base is indicated by lack of any storm- or wave-induced sedimentary structures and the interbedding with dolomitic siltstone of LF16. Likely depositional mechanisms include hemipelagic settling and low-density turbidity currents (Wignall, 1994) in deep subtidal to slope environments (Fig. 7).

4.4.5. LF18: mass-flow breccia (sand-sized/ > sand-sized)

This lithofacies occurs as centimeter- to meter-thick intervals in the Barney Creek Formation and Reward Dolostone and is typically interbedded with other facies from FA4. Slope breccias interrupt the deposition of LF19 and LF16 facies. Mass-flow breccias are composed of medium to dark grey (rare black) grainstones, conglomerates, and breccias. They are matrix- or clast-supported, mostly polymict but sometimes monomict, and moderately (rare) to very poorly sorted. The clast size is either dominated by granule- to cobble-sized clasts (Fig. 6C) or sand-sized grains (Fig. 6D), which we distinguish in logs. The sand-sized subfacies is similar to dolarenite (LF14) with the main differences being polymict composition and generally larger grainsize. The tabular- to equant-shaped clasts of mass-flow breccias typically show no fitting. Compositionally, this facies is dominated by well-rounded to very angular carbonate clasts; however, angular dolomitic siltstone clasts and quartz grains may also occur. Interstitial pyrite and base metal sulfides may occur. Mass-flow breccias are very thinly to medium bedded, sometimes massive. They are typically ungraded but may also show normal or inverse grading.

The lack of fitting, unsorted clasts, and variable degree of roundness, as well as interbedding with rhythmite (LF19) and silty dolarenite/dolomitic siltstone (LF16) indicate a gravity-flow origin (e.g., Coniglio and Dix, 1992; Flügel, 2004; James and Jones, 2016 p. 2016). Mass-flow breccias were likely generated by gravitational collapse and coherent mass wasting of lithified platform margin and upper slope deposits (Playton et al., 2010) and subsequent down-slope transport and re-sedimentation (Fig. 7). Whereas polymict deposits suggest mixing of clasts from multiple platform margin environments (e.g., shoals, biological buildups) and/or upper slope environments, monomict deposits had only one source area and are typically the result of erosion and re-deposition of upper slope carbonates (Coniglio and Dix, 1992). Variability in clast size, grading (un-, normal-, or inverse graded), and bedding (bedded or massive) suggest that transport mechanisms differed for individual beds and likely included coarse-grained turbidity currents and debris flows for the larger than sand-sized subfacies, and fine-grained turbidity currents and grainflows for the sand-sized subfacies. Therefore, the origin of the latter is similar to dolarenite (LF14) beds.

4.4.6. LF19: rhythmite

Rhythmites, characterized by alternation of darker and lighter grey laminae and beds of similar thickness, can occur as meter- to decimeter-thick intervals in the undifferentiated Barney Creek Formation. This lithofacies is composed of dark grey (rare medium grey), very fine

to fine dolarenite (Fig. 6F). It is typically thickly laminated to thinly bedded. Individual laminae and beds can have an erosional base. They are massive or have an internal, mm-scale, planar-parallel lamination with fining-upward. Slump folds (Fig. 6F) and cm-scale growth faults are common.

The absence of wave or current-induced structures indicates deposition below storm wave base. Furthermore, common slump folds suggest deposition onto an inclined sea floor such as a slope (Fig. 7). The sediments were likely deposited out of suspension, either as pelagic and hemipelagic fallout from the water column or as sediment-sea-water-mixtures that moved downslope as dilute allodapic flows (e.g., Coniglio and Dix, 1992; Playton et al., 2010; James and Jones, 2016 p. 214). Fallout deposition can occur after storms, tides, or currents transported fine material from the platform interior or platform margin into deeper water settings. If these suspensions are dense enough they can transform into dilute allodapic flows. The occasionally observed sharp, erosional lower contacts, and normal grading support the interpretation of deposition out of allodapic flows such as dilute turbidity currents (e.g., Cook and Mullins, 1983).

5. Discussion

5.1. Stratigraphic evolution

The three studied drill cores intersect the middle McArthur Group in different tectonic settings. GRNT-79-7 intersects the Barney Creek Formation in the Glyde sub-basin (Fig. 1). In contrast, Leila Yard 1 and Lamont Pass 3 intersect the succession on the adjacent paleohigh to the north (although this area is marked by small, higher order sub-basins). As the Barney Creek Formation was the drilling target, only Lamont Pass 3 intersects a significant stratigraphic range below the Barney Creek Formation. Therefore, our stratigraphic interpretation only considers the vertical evolution for these units.

The Tooganinie Formation is the oldest intersected stratigraphic unit, cored below ca. 1045 m in Lamont Pass 3 (Fig. 8). The intersected thickness is ca. 229 m, but its base was not drilled. Consistent with general descriptions of this unit by Jackson et al. (1987), our log shows that it is distinguished by interbedding of peritidal dolostones, mostly stromatolites (LF11), and green siltstones (LF1; Fig. 8). In Lamont Pass 3, the top shoals from subtidal stromatolites to sabkha environments, as indicated by increasing abundance of red siltstone with anhydrite (LF1). Therefore, the Tooganinie Formation represents a regressive transition into the Leila Sandstone and Myrtle Shale.

The Leila Sandstone in Lamont Pass 3 is 11 m thick (Fig. 8). It is an immature, medium- to coarse-grained sandstone with abundant siltstone (LF1) rip up clasts, siltstone laminae, and mudcracks. Therefore, this sandstone was likely deposited in supratidal environments and represents continuation of upward shoaling.

Eighty-two meters of the Myrtle Shale were intersected in Lamont Pass 3. We interpret the Myrtle Shale to represent a mosaic of sabkha environments, dominated by interbedding of red and green siltstone (LF1). This drill core records a gradual transition from the Myrtle Shale into the overlying Emmerugga Dolostone, marked by two conglomerate cycles. Each conglomerate bed is limited to siltstone clasts in the lower half but carbonate clasts (LF4 and LF8) come in towards the top. This suggests retrogradation of the shoreline and re-working of inter- to supratidal carbonate environments. The basal carbonate bed of the Emmerugga Dolostone is a dolarenite breccia dominated by carbonate clasts with a silty matrix, again indicating a gradual transition.

The Emmerugga Dolostone in Lamont Pass 3 is an ~80 m-thick interval dominated by subtidal stromatolites (LF11) and shallow subtidal bedded dolarenites (LF4; Fig. 8), representing flooding of the Myrtle Shale sabkha environments. The stromatolites are commonly entirely brecciated, grow on brecciated surfaces and/or are brecciated at the top. The abundant brecciation may indicate regular storm activity and that stromatolite bioherms formed barriers that allowed dolarenite and

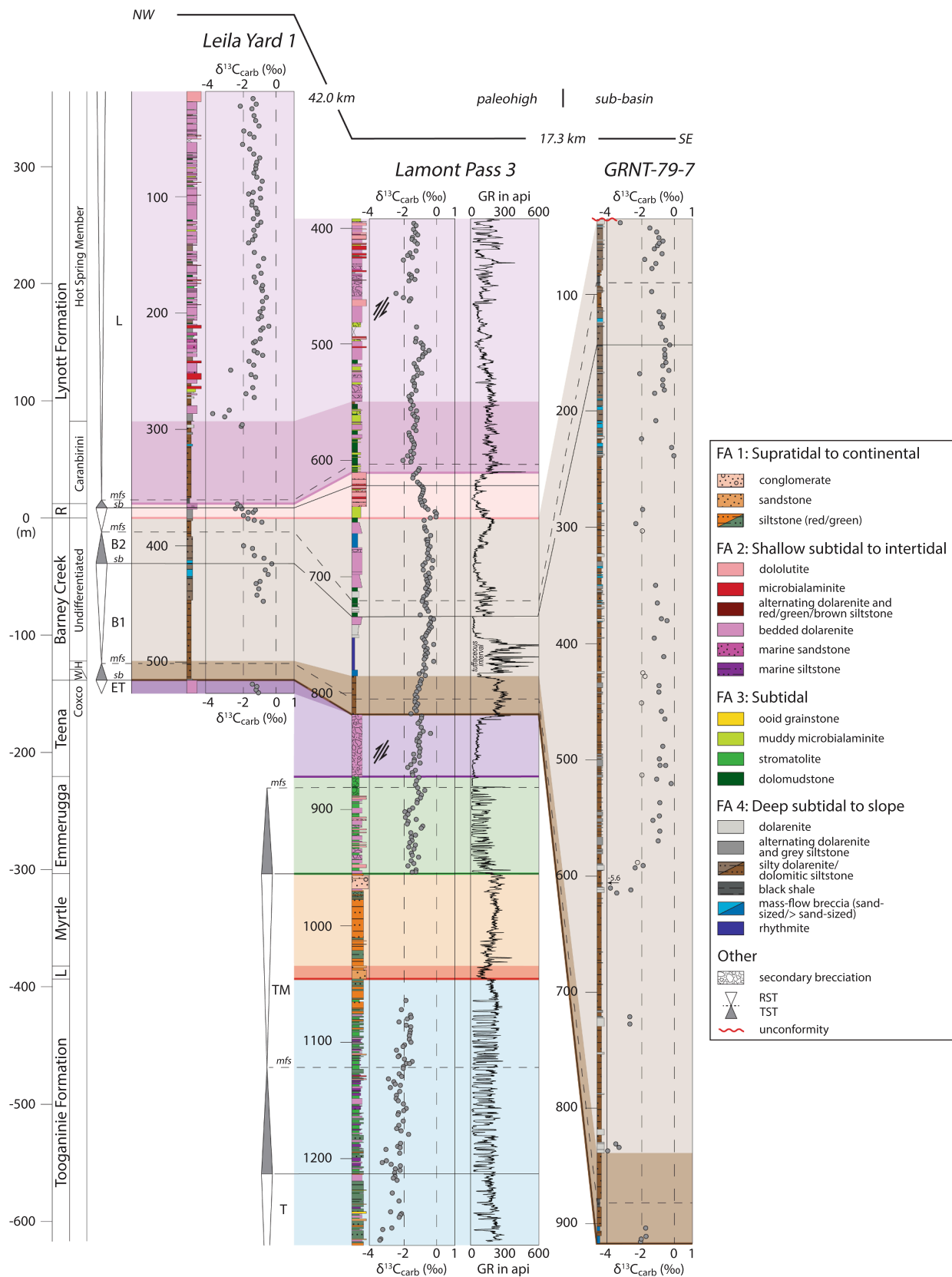


Fig. 8. Litho-, sequence, and carbon isotope stratigraphy of drill cores Leila Yard 1, Lamont Pass 3, and GRNT-79-7 (see Fig. 1 for location). Lower resolution carbon isotope record in the Barney Creek Formation in Leila Yard 1 and GRNT-79-7 is due to scarcity of carbonate beds. Unfilled circles in GRNT-79-7 reflect altered samples with very low $\delta^{18}\text{O}_{\text{carb}}$ values (see Fig. 10). Abbreviations: mfs = maximum flooding surface; sb = sequence boundary.

dololite deposition in protected low-energy environments. We choose the base of a ca. 60 m thick, faulted and brecciated dolarenite interval as the boundary with the overlying Teena Dolostone (Fig. 8). However, a clear facies distinction between these units is not observable in Lamont Pass 3. Furthermore, a distinction between the Mara Dolostone and Mitchell Yard Member in the Emmerugga Dolostone cannot be made in Lamont Pass 3. This ambiguity highlights the need for careful stratigraphic studies and potential revision of stratigraphic nomenclature in the southern McArthur Basin considering complex paleotopography inherited by the underlying Tawallah Group, lateral facies changes, and diachronous deposition.

The overlying Teena Dolostone is only represented by the brecciated dolarenite succession in Lamont Pass 3. At least part of this brecciation is due to faulting, accompanied by strong pyrite and weak base metals mineralization. The uppermost Teena Dolostone is intersected in Leila Yard 1 and comprises shallow subtidal to intertidal facies (FA2). The occurrence of Coxco needles indicates that the Coxco Member is developed in this area. In contrast, it is not developed ca. 42 km to the southeast in Lamont Pass 3 (Fig. 8). GRNT-79-7 does not intersect this part of the stratigraphy but a study by Davidson and Dashlooty (1993) demonstrated that the Coxco Member is developed in the Glyde sub-basin.

The transition into the overlying Barney Creek Formation coincided with fault reactivation, which led to renewed extension of the basin and the formation or reactivation of numerous sub-basins and paleohighs (McGoldrick et al., 2010). This episode of extension led to flooding of peritidal facies of the Teena Dolostone in Leila Yard 1 and Lamont Pass 3, and deposition of deep subtidal to slope facies (FA4) of the Barney Creek Formation in all three drill cores (Fig. 8).

The W-Fold Shale is a transitional unit that is only developed as a one meter-thick interval of alternating dolarenite and dark grey siltstone (LF15) in Leila Yard 1. The following HYC Pyritic Shale Member is a bituminous and pyritic dolomitic siltstone (LF16) in all three drill cores, independent of a paleohigh or sub-basin setting. This lithological uniformity testifies to significant deepening across the entire studied part of the basin. In addition, the sedimentological composition of the HYC Pyritic Shale Member in the three drill cores presented here is comparable to the correlative mineralized interval at McArthur River (Large et al., 1998) and a studied core located approximately 23 km southwest of McArthur River (Bull, 1998). Despite the similar sedimentological composition, our transect shows a significantly thicker HYC Pyritic Shale Member in the sub-basin intersection in GRNT-79-7 (78 m) compared to the paleohigh intersections in Lamont Pass 3 (33 m) and Leila Yard 1 (17 m). Furthermore, a 7 m-thick black shale (LF17) interval occurs in GRNT-79-7. These observations are consistent with the generally deeper depositional environment in the sub-basin.

The overlying undifferentiated Barney Creek Formation is marked by significant lateral thickness changes, from less than 200 m on the paleohigh to more than 800 m in the sub-basin (Fig. 8). Furthermore, the Barney Creek Formation in GRNT-79-7 is truncated by the sub-Cambrian unconformity, and therefore the current thickness of the Barney Creek Formation in this sub-basin section is a minimum estimate of its original thickness. This lateral thickness difference indicates significant fault-controlled subsidence in the sub-basin. The undifferentiated Barney Creek Formation is mostly composed of silty dolarenite/dolomitic siltstone (LF16) but compared to the HYC Pyritic Shale Member has a higher carbonate content, is less bituminous, and contains abundant carbonate gravity flow deposits (LF14, LF15, LF18). Mass-flow breccias (LF18) are particularly common in the middle and upper part of the undifferentiated Barney Creek Formation (Fig. 8). Taken together, these features indicate general shoaling upward. The undifferentiated Barney Creek Formation is dominated by dolomitic siltstone in Leila Yard 1 and GRNT-79-7. However, in Lamont Pass 3, located close to the Emu Fault (Fig. 1), the upper part comprises subtidal (FA3) to shallow subtidal (FA2) carbonate facies (Fig. 8). This indicates that while rapid early subsidence occurred across the entire

studied part of the Batten Fault Zone at the onset of HYC Pyritic Shale Member deposition, subsidence rates of the eastern part of this particular paleohigh decreased during deposition of the upper undifferentiated Barney Creek Formation and allowed the establishment of subtidal to shallow subtidal environments.

The overlying formations are only preserved in the two drill cores from the paleohigh. The Reward Dolostone shows a continuation of the general shoaling observed in the undifferentiated Barney Creek Formation. It thickens from 13 m in Leila Yard 1 on the northwestern side of the paleohigh to 40 m in Lamont Pass 3 in the southeast. This thickness increase is accompanied by a facies shift from mostly deep subtidal carbonate facies to mostly shallow subtidal to intertidal carbonate facies (Fig. 8). Therefore, Lamont Pass 3 continues to record shallower depositional environments (as observed in the upper undifferentiated Barney Creek) than Leila Yard 1.

The Caranbirini Member of the Lynott Formation is ca. 70 m thick in both Leila Yard 1 and Lamont Pass 3 (Fig. 8). It records a shift to deeper depositional environments, indicated by the deposition of deep subtidal to slope (FA4) black shale (LF17) facies and dolomitic siltstone (LF16) in Leila Yard 1 and subtidal (FA3) muddy microbialaminite (LF11) and dolomudstone (LF13) in Lamont Pass 3. This means, although the Caranbirini Member shows general deepening, a lateral gradient from deeper environments in the northwest to shallower environments in the southeast is preserved on this paleohigh. Therefore, the lateral gradient that is already present in the upper Barney Creek Formation continues through to the Caranbirini Member.

The Hot Spring Member of the Lynott Formation is composed of shallow subtidal to intertidal facies (FA2) in both Leila Yard 1 and Lamont Pass 3 (Fig. 8). A lateral depth gradient is not observable. The total thickness of this member is unknown as both cores are collared in the Hot Spring Member.

5.2. Sequence stratigraphy

We have identified four complete and two partial T-R sequences over the studied interval. The upper part of the RST of sequence T in the Tooganinie Formation is cored in Lamont Pass 3 (Fig. 8). A MRS at the top of a red and green siltstone bed coincides with a shift in the gamma pattern and marks the top of a succession dominated by supratidal siltstone.

The overlying TST of sequence TM is marked by regular interbedding of subtidal stromatolites (LF11) and shallow subtidal to supratidal siltstones (LF6, LF1), producing a characteristic pattern of alternating low and high gamma ray readings (Fig. 8). The stromatolite/siltstone ratio generally increases upsection in the TST, indicating flooding, and the TST culminates in a MFS within a thick stromatolite interval (Fig. 8). The following RST comprises the uppermost Tooganinie Formation, where it is marked by decreasing stromatolite/siltstone ratio, the shallow marine to supratidal Leila Sandstone, and sabkha facies of the Myrtle Shale. The top of sequence TM coincides with the boundary of the Myrtle Shale to the Emmerugga Dolostone (Fig. 8). We identify this surface as a MRS.

Southgate et al. (2000) and Jackson et al. (2000) describe a sequence boundary at the base of the Leila Sandstone as 'incision surface that truncates subtidal green shale of the Tooganinie Formation' and separates shallower facies above from deeper facies below. Due to rare outcrops, they only observed the Leila-Tooganinie contact in one location near the McArthur River deposit. In Lamont Pass 3, the Tooganinie-Leila contact is not associated with significant incision. It is a scour surface marked by shale/siltstone rip up clasts in the lowermost 5 cm of the Leila Sandstone, which can be explained by deposition of the sandstone on top of unlithified shale/siltstone. We interpret this surface as a regressive surface of marine erosion (RSME), which is a highly diachronous surface associated with a minor time gap formed as a scour zone during base level fall (Plint, 1988). Further support for an overall gradual transition instead of a major unconformity representing

a sequence boundary comes from shale/siltstone beds and rip up clasts throughout the Leila Sandstone in Lamont Pass 3. Furthermore, the uppermost Tooganinie Formation already contains red siltstone with anhydrite nodules, as typical for the overlying Myrtle Shale in Lamont Pass 3.

The overlying TST of sequence ET culminates in a MFS marked by a thin dolomudstone (LF13) bed and a corresponding peak in the gamma ray log (Fig. 8). The following RST is capped by a MRS at the top of the Teena Dolostone, which comprises bedded dolarenite (LF4) in both Lamont Pass 3 and Leila Yard 1. Using the gamma ray log available from Lamont Pass 3, the MRS could be placed slightly lower at the inflection point of increasing gamma ray values. However, we choose the facies change as MRS as this entire interval is brecciated in Lamont Pass 3 (post-depositional), making it difficult to interpret the gamma ray log.

Southgate et al. (2000) and Jackson et al., 2000 describe a karst surface at the base of the Teena Dolostone (i.e. in the middle of our sequence ET), which they observed in one location. This proposed sequence boundary is also used as base for the River Supersequence (a 2nd-order sequence defined on the Lawn Hill Platform in Queensland) in the southern McArthur Basin (Jackson et al., 2000). In Lamont Pass 3, the transition between the Emmerugga and Teena dolostones is transitional and we do not observe an unconformity. Furthermore, the entire Teena Dolostone is faulted, and as a result, is brecciated (Fig. 8) and mineralized with pyrite and minor base metal sulfides. Future studies and a more regional assessment are required to better understand this contact.

The overlying Barney Creek Formation comprises two sequences, herein called B1 and B2. Sequence B1 comprises the W-Fold Shale, HYC Pyritic Shale Member, and roughly the lower half of the undifferentiated Barney Creek Formation (Fig. 8). Although slightly thicker in the sub-basin intersected in GRNT-79-7, the TST of B1 is generally only a few meters thick in the studied drill cores (Fig. 8). On the paleohigh, the MFS sits within an interval of bituminous dolomitic siltstone (LF16) of the middle HYC Pyritic Shale Member, marked by a peak in the gamma ray log in Lamont Pass 3, and elevated pyrite abundance in Leila Yard 1. In the sub-basin section of GRNT-79-7, it sits within a black shale (LF17) interval in the middle HYC Pyritic Shale Member. As discussed above, the HYC Pyritic Shale Member records significant flooding across the entire studied part of the basin, not only in sub-basins. Strata of the RST shoal to shallow subtidal facies in the undifferentiated Barney Creek in Lamont Pass 3. The RST is capped by a MRS, which is associated with a sharp increase in gamma ray values and a shift in $\delta^{13}\text{C}_{\text{carb}}$ from increasing to decreasing values (Fig. 8). In contrast to Lamont Pass 3, the RST does not record shoaling to shallow subtidal environments in Leila Yard 1 and GRNT-79-7. Here, the MRS sits within silty dolarenite (LF16) turbidite deposits (Fig. 8), which is a typical location for the MRS in deeper water settings (Embry and Johannessen, 2017). Gamma ray data are not available to identify the exact stratigraphic location of the MRS. However, using a $\delta^{13}\text{C}_{\text{carb}}$ shift associated with the MRS in Lamont Pass 3 as a chronostratigraphic marker, the MRS can be identified in these holes (Fig. 8).

Sequence B2 comprises the upper undifferentiated Barney Creek Formation and the Reward Dolostone (Fig. 8). The TST records less relative deepening of depositional environments across the studied area than the TST of B1. In Leila Yard 1 and GRNT-79-7, silty dolarenite gives way to pyritic and bituminous dolomitic siltstone and Lamont Pass 3 records deepening from shallow subtidal bedded dolarenite (LF4) to subtidal dolomudstone (LF13). The MFS sits within a pyritic black shale (LF17) interval in the sub-basin succession of GRNT-79-7 and is associated with a $\delta^{13}\text{C}_{\text{carb}}$ shift from decreasing to increasing values. This shift also occurs in Lamont Pass 3 and helps to identify the MFS within an interval of generally high gamma ray values (Fig. 8). In Leila Yard 1, the MFS is expressed as pyritic dolomitic siltstone. The RST of sequence B2 is marked by shoaling from slope facies (Leila Yard 1) and subtidal facies (Lamont Pass 3) of the undifferentiated Barney

Creek Formation to shallow subtidal and intertidal facies of the upper Reward Dolostone in both cores. In GRNT-79-7, the RST is truncated by the Cambrian unconformity (Fig. 8). We place the sequence boundary in the upper Reward Dolostone (but not the top), at the onset of rising gamma ray values in Lamont Pass 3. We identify the sequence boundary as MRS is Leila Yard 1 but it is unclear whether it is a MRS or an unconformable shoreline ravinement surface in Lamont Pass 3. However, we do not see evidence for significant truncation and erosion as expected for an unconformable shoreline ravinement surface. In fact, the $\delta^{13}\text{C}_{\text{carb}}$ values change gradually across the boundary into the Caranbirini Member, which is consistent with a gradual change (i.e., MRS) instead of a hiatus. As the Reward-Lynott contact has previously been described as a locally developed unconformity (Ahmad et al., 2013), a regional scale perspective is required to better understand where this contact is developed as unconformity.

Sequence L comprises the Caranbirini and Hot Spring members of the Lynott Formation. A thin TST is developed in the lowermost Caranbirini Member and culminates in a MFS expressed as pyritic black shale (LF17) in Leila Yard 1 and a dolomudstone (LF13) marked by a gamma ray peak in Lamont Pass 3 (Fig. 8). Although Leila Yard 1 records deeper depositional environments during deposition of the Caranbirini Member, including the lower RST of sequence L, shoaling upwards to shallow sub- to intertidal environments in the Hot Spring Member is recorded in both drill cores (Fig. 8).

The Barney Creek Formation and the Caranbirini Member are lithologically similar and hence may be difficult to distinguish. Sequence stratigraphy can be used to distinguish these two units. Whereas the Barney Creek Formation comprises one full sequence (B1) and the TST and lower RST of a second sequence (B2), the Caranbirini Member only consists of one TST and part of an RST (L).

5.3. Sequence stratigraphic correlation with Lawn Hill Platform

The late Paleoproterozoic succession in Queensland is divided into seven 2nd-order supersequences (Southgate et al., 2000). Geochronological constraints indicate that middle McArthur Group equivalent strata is represented by the River Supersequence, which can be subdivided into eight 3rd-order sequences (Fig. 9; Krassay et al., 2000). We present a possible correlation of these sequences with our interpreted sequence stratigraphic framework in the southern McArthur Basin (Fig. 9). Correlation of these sequences assumes that they formed synchronously, which means that the interplay of accommodation space and sedimentation was controlled by the same mechanism in both areas or that both at least shared the same allostratigraphic control. Correlation of strata in these areas is complicated by the complex tectonic history of the north Australian Proterozoic basins. Specifically, seismic sections indicate onlap of Lawn Hill strata onto the southern Murphy inlier (Southgate et al., 2000), which separates the southern McArthur Basin from the Lawn Hill Platform. Furthermore, only the upper three sequences of the River Supersequence are preserved on the northern Lawn Hill Platform (Southgate et al., 2000; Krassay et al., 2000). These observations indicate that the Murphy inlier was a paleohigh at the time of deposition, separating depocenters on both sides. Nevertheless, as both successions were deposited in less than ca. 15 million years and have a comparable number of sequences with similar thicknesses, it is reasonable to assume more or less synchronous deposition and to attempt to correlate the sequence stratigraphic records from both areas (Fig. 9).

Previous workers have proposed different stratigraphic positions for the base of the River Supersequence in the southern McArthur Basin (Fig. 9). For example, the unconformity described by Southgate et al. (2000) from the base of the Leila Sandstone has been used as base of the River Supersequence (Southgate et al., 2000; McGoldrick et al., 2010). However, we identify this surface as a RSME and not as a sequence boundary. Another possibility was suggested by Jackson et al. (2000) who described a karst surface at the base of the Teena Dolostone and

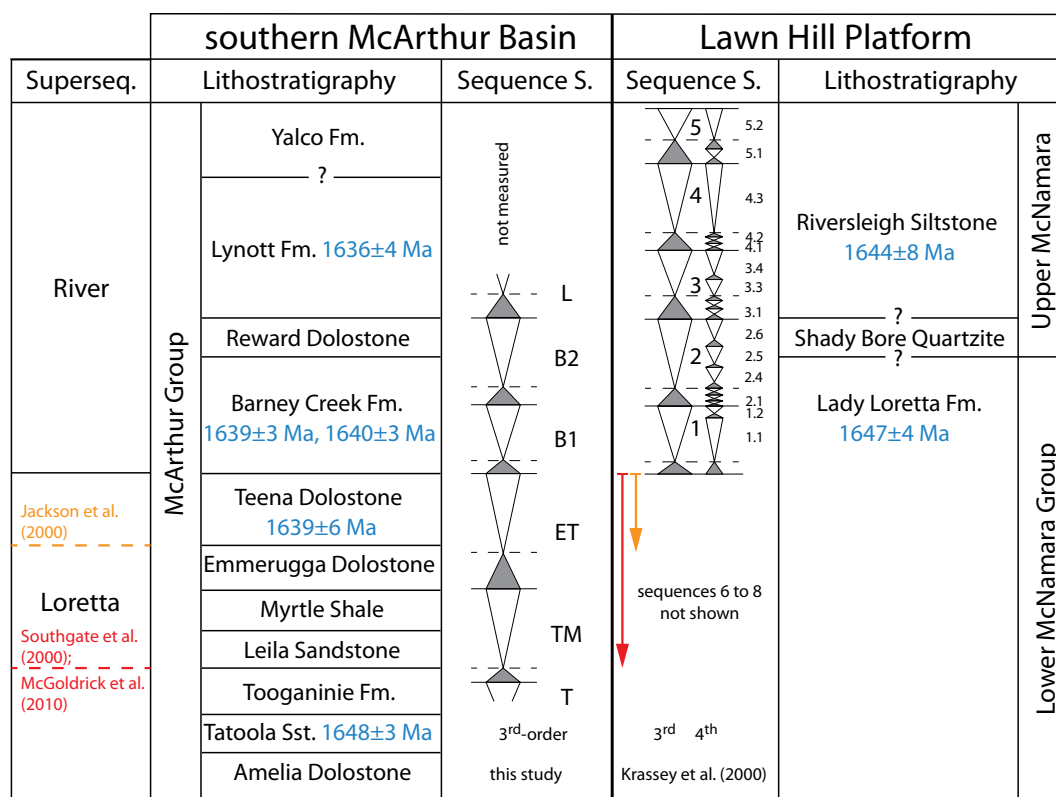


Fig. 9. Possible correlation of 3rd-order sequences of the River Supersequence in the southern McArthur Basin (this study) and the Lawn Hill Platform (Krassey et al., 2000). This correlation is based on placing the River Supersequence boundary at the Teena-Barney Creek transition. Previous interpretations for the base of the Supersequence include the base of the Teena Dolostone (orange dashed line and arrow; Jackson et al., 2000) and the base of the Leila Sandstone (red dashed line and arrow; Southgate et al., 2000; McGoldrick et al., 2010). The new correlation is permissible by existing geochronological constraints (Page and Sweet, 1998; Page et al., 2000).

used this sequence boundary as the base for the River Supersequence. Although future work is required to better understand this contact, we do not recognize a karst surface or sequence boundary between the Emmerugga and Teena dolostones in Lamont Pass 3. Therefore, we offer an alternative interpretation for the base of the River Supersequence in the southern McArthur Basin.

Second-order sequences such as the River Supersequence are thought to have a duration between 3 and 50 million years (Vail et al., 1991) and are mostly controlled by regional tectonics (e.g., Nystuen, 1998; Embry, 2009). The boundaries are marked by a change of the tectonic regime (Embry, 2009) and significant deepening and erosion in different parts of the basin. In the middle McArthur Group, the most significant tectonic activity occurred at the Teena-Barney Creek transition (e.g., McGoldrick et al., 2010). Movement along broadly north-south striking strike-slip faults led to significant sub-basin deepening in some areas and significant uplift and erosion in other areas. For example, GRNT-79-7 records 900 m of deep subtidal to slope facies of the Barney Creek Formation (Fig. 8) deposited in the Glyde sub-basin along the western side of the Emu Fault and indicates significant subsidence. In contrast, deposition of mass-flow breccias (Cooley Dolostone Member), for example at McArthur River (Williams, 1978; Ireland et al., 2004a), were shed from uplifted fault blocks along the Emu Fault and indicate erosion. About 10 km south of the McArthur River deposit, a karst surface separates the lower Emmerugga Dolostone from the Reward Dolostone (Walker et al., 1983). This surface could have formed any time between the Emmerugga and Reward dolostones; however, we suggest it formed at the top of the Teena Dolostone, leading to truncation of the Teena and upper Emmerugga dolostones and non-deposition of the Barney Creek Formation. This is consistent with the general occurrence of clasts of Teena and Emmerugga dolostones in the Cooley Dolostone Member (Williams, 1978; Jackson et al.,

1987). Based on these observations, we suggest that the base of the River Supersequence coincides with the Teena-Barney Creek transition in the southern McArthur Basin. Following this assumption, we correlate previously described 3rd-order sequences from the Lawn Hill Platform (Krassey et al., 2000) with 3rd-order sequences described in this contribution (Fig. 9).

The base of the River Supersequence sits within the upper portion of the 1647 ± 4 Ma Lady Loretta Formation on the Lawn Hill Platform (Bradshaw et al., 2000; Krassey et al., 2000 Fig. 9). Following our proposed position of the base of the River Supersequence in the southern McArthur Basin, the 1640 ± 3 Ma Barney Creek Formation correlates with the upper Lady Loretta Formation (Fig. 9). The 1636 ± 4 Ma Lynott Formation in the McArthur Basin may represent sequences 3–4 of the River Supersequence, which belong to the 1644 ± 8 Ma Riversleigh Siltstone on the Lawn Hill Platform.

The sequence stratigraphic correlation proposed herein is only a first attempt to reconstruct a regional 3rd-order sequence stratigraphic framework. A more precise geochronological framework and extended carbon isotope record is required to test this correlation and expand it to other areas of the greater McArthur Basin (e.g., Birrindudu Basin, Walker Fault Zone).

5.4. Carbon isotope chemostratigraphy

Carbon and oxygen isotope ratios show no systematic relationship for Lamont Pass 3 and Leila Yard 1 (Fig. 10), indicating a lack of strong secondary alteration. In contrast, carbon and oxygen isotopes in GRNT-79-7 show a weak positive correlation (Fig. 10), suggesting that some samples experienced secondary alteration, which may be due to meteoric waters (Allan and Matthews, 1982). Furthermore, a small subset (n = 6) of samples from this core have very light $\delta^{18}\text{O}_{\text{carb}}$ values

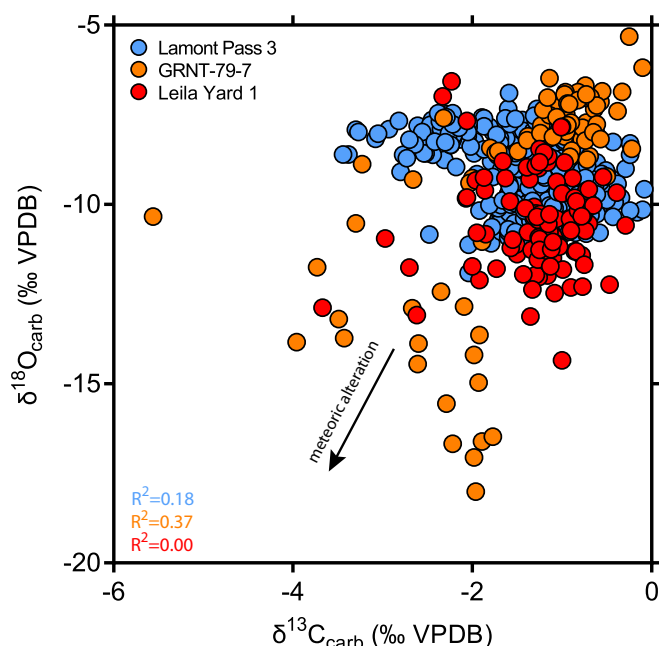


Fig. 10. Carbon and oxygen isotope cross-plot of all data from Leila Yard 1 ($n = 100$), Lamont Pass 3 ($n = 305$), and GRNT-79-7 ($n = 80$). Samples from GRNT-79-7 with $\delta^{18}\text{O}$ values below ca. -15‰ reflect significant meteoric alteration and are only shown by unfilled circles in Fig. 5.

(< -15‰ ; Fig. 10), likely indicating that they experienced significant alteration. These samples are indicated by open circles in Fig. 8 and not further considered. As only samples from GRNT-79-7 experienced weak alteration, we generally consider the carbon isotope data set to be a faithful record of the primary carbon isotopic composition of the depositional environment.

Carbon isotope values of mostly carbonate lithofacies (only 15 samples were dolomitic siltstone; see Methods) show significant and systematic variation in the middle McArthur Group (Fig. 8). In Lamont Pass 3, $\delta^{13}\text{C}_{\text{carb}}$ values gradually increase throughout the Tooganinie Formation from ca. -3.5‰ to ca. -2‰ . Due to absence of carbonate beds, we were not able to produce a $\delta^{13}\text{C}_{\text{carb}}$ record from the overlying Leila Sandstone and Myrtle Shale. However, values continue to increase upsection through the Emmerugga and Teena dolostones to a maximum of ca. 0‰ in the middle Barney Creek Formation, followed by an upsection decrease to ca. -2‰ to -1.5‰ in the Reward Dolostone and Lynott Formation (Fig. 8).

This trend generally does not correspond to major changes in the depositional settings throughout the succession. Although shoaling to inter- to supratidal environments in the upper Tooganinie Formation is accompanied by a trend towards higher $\delta^{13}\text{C}_{\text{carb}}$, the isotopic ratio is much lower as reported from modern and ancient sabkha environments (Stiller et al., 1985; Schmid, 2017). Furthermore, the highest $\delta^{13}\text{C}_{\text{carb}}$ values are recorded by the Barney Creek Formation, which reflects the deepest depositional environments in the middle McArthur Group. Shoaling upward, as recorded in the Reward Dolostone and Hot Spring Member is accompanied by decreasing $\delta^{13}\text{C}_{\text{carb}}$. A lateral isotope gradient across the presented ca. 60 km transect, spanning a sub-basin and paleohigh environment, is also not observable. These observations suggest that the 3.5‰ variation in the middle McArthur Group does not record vertical or horizontal isotope gradients in the basin.

In contrast, we attribute a subordinate $\delta^{13}\text{C}_{\text{carb}}$ trend of ca. $1\text{--}2\text{‰}$ in carbonate lithofacies of the Barney Creek Formation (Fig. 8) to a depth gradient in the dissolved inorganic carbon reservoir of the sampled water body. In Lamont Pass 3, deepening in the basal Barney Creek Formation corresponds to decreasing $\delta^{13}\text{C}_{\text{carb}}$ values from -1 to -1.5‰ at the MFS of sequence B1. The following RST is marked by

increasing $\delta^{13}\text{C}_{\text{carb}}$ to maximum values around 0‰ at the sequence boundary. The overlying TST of sequence B2 shows decreasing values to ca. -1‰ , followed by values around -0.5‰ in the RST of the upper Barney Creek Formation (Fig. 8).

Although the observed isotopic range of $1\text{--}2\text{‰}$ in the Barney Creek Formation in Lamont Pass 3 is relatively low, comparable values and trends are observable in the other two drill cores (Fig. 8). In GRNT-79-7, $\delta^{13}\text{C}_{\text{carb}}$ values decrease from -2‰ to ca. -4‰ in the lower Barney Creek Formation (due to lack of carbonate beds only a low resolution data set was produced), followed by an upsection trend of increasing values to ca. 0‰ at the B2 sequence boundary. The TST of sequence B2 is marked by decreasing values to ca. -2‰ around the MFS. However, the MFS itself was not analyzed because it does not sit within a carbonate interval. The preserved lower part of the RST shows slightly increasing $\delta^{13}\text{C}_{\text{carb}}$ values (Fig. 8). Importantly, the described trends in GRNT-79-7 occur in stratigraphically thicker intervals compared to Lamont Pass 3, reflecting significantly greater sedimentation rates in the sub-basin. Due to the lack of carbonate beds, we only present $\delta^{13}\text{C}_{\text{carb}}$ data from the middle portion of the Barney Creek Formation in Leila Yard 1. Carbon isotope ratios increase from ca. -1‰ in the upper RST of sequence B1 to 0‰ at the B2 sequence boundary. This maximum is followed by a decline to -2‰ in the TST of sequence B2.

The Reward Dolostone also shows a $1\text{--}2\text{‰}$ trend in $\delta^{13}\text{C}_{\text{carb}}$. In Lamont Pass 3, $\delta^{13}\text{C}_{\text{carb}}$ values sharply increase from ca. -1 to 0‰ in the lower Reward Dolostone, followed by a gradual decline to ca. -1.5‰ throughout the Reward Dolostone (Fig. 8). A similar trend is recorded by the Reward Dolostone in Leila Yard 1. $\delta^{13}\text{C}_{\text{carb}}$ values first increase from -2‰ to -1‰ and then decline to -2.5‰ . In Leila Yard 1 this trend is condensed due to lower sedimentation rates and systematically offset towards lighter values by ca. 1‰ . This is consistent with a surface-to-depth isotope gradient in the sampled water body, comparable to the trend in the Barney Creek Formation.

In summary, carbon isotope data show a systematic 3.5‰ trend in carbonate facies of the middle McArthur Group. This trend does not correspond to the depositional environment of the stratigraphic units, suggesting it can be used for basin-wide correlation. Subordinate $\delta^{13}\text{C}_{\text{carb}}$ trends of $1\text{--}2\text{‰}$ in the Barney Creek Formation and Reward Dolostone correspond to trends in relative water depth and likely reflect an isotope gradient in the sampled water mass. Future carbon isotope work on these units in other locations is required to test whether these low-amplitude shifts in $\delta^{13}\text{C}_{\text{carb}}$ are a basin-wide signal and can be used for basin-scale correlation. However, given that we observe these trends in a 60 km transect across a sub-basin and paleohigh seem to suggest this.

5.5. Chemostratigraphic correlation with North China Craton

The Changcheng and Nankou groups on the North China Craton represent a late Paleo-Mesoproterozoic mixed siliciclastic-carbonate rift to drift succession (Chu et al., 2007; Meng et al., 2011). Marine carbonate rocks of the Tuanshanzi Formation comprise the upper part of the Changcheng Group and are dated by an interbedded tuff bed that yielded a zircon $^{207}\text{Pb}/^{206}\text{Pb}$ age of 1637 ± 15 Ma (Zhang et al., 2013). The overlying Dahongyu Formation of the Nankou Group comprises basal sandstones, overlain by carbonate rocks, and an interbedded tuff yielded a SHRIMP U-Pb age of 1622 ± 23 Ma (Lu et al., 2008) and a single zircon U-Pb age of 1625 ± 6 Ma (Lu and Li, 1991). These formations are thus the same age as the middle McArthur Group, within analytical uncertainty (Fig. 11).

Carbon isotope chemostratigraphic data of the Tuanshanzi and Dahongyu formations were previously reported by Chu et al. (2007) and data from the Tuanshanzi Formation display a strikingly similar isotopic range and trend to our data from the middle McArthur Group (Fig. 11). Given the comparable age, within analytical uncertainty, we propose that the Tuanshanzi Formation is equivalent to the interval from the Tooganinie to Lynott Formation in the southern McArthur

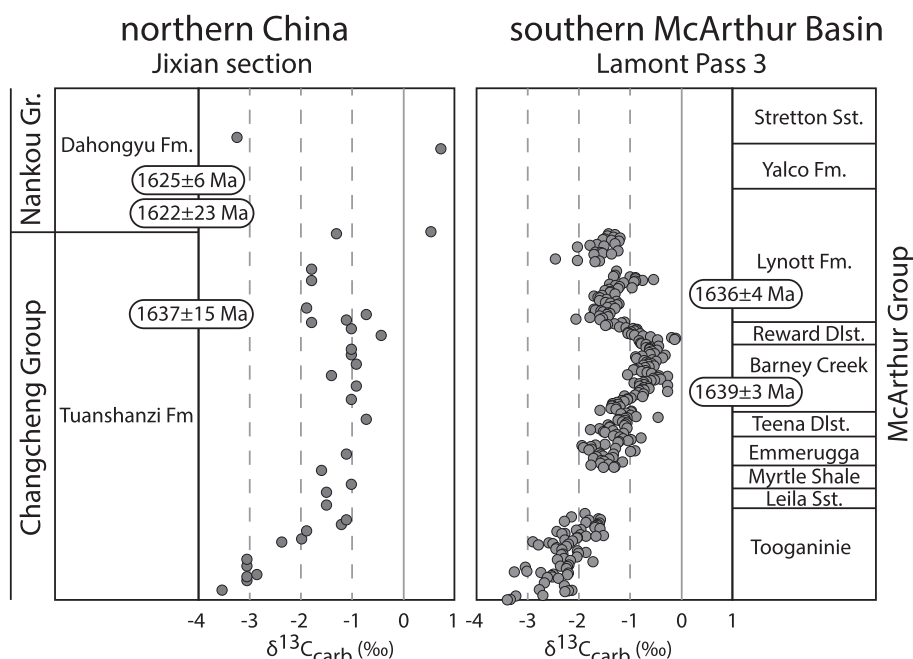


Fig. 11. Carbon isotope chemostratigraphic records of the Jixian section on the North China Craton (least altered samples; [Chu et al., 2007](#)) and the middle McArthur Group in Lamont Pass 3 (this study). Radiometric ages are from [Lu and Li \(1991\)](#), [Lu et al. \(2008\)](#), [Zhang et al. \(2013\)](#), [Page and Sweet \(1998\)](#), and [Page et al. \(2000\)](#).

Basin. The preservation of a comparable $\delta^{13}\text{C}_{\text{carb}}$ record on two different cratons indicates that the carbon isotope curve from the middle McArthur Basin is at least a basin-wide record. If both successions were deposited in different basins, the presented data could be used to construct an age-calibrated global carbon isotope record for this time.

5.6. Implications for exploration

Our sedimentological and stratigraphic evaluation of the Barney Creek Formation, the most important Zn-Pb host unit in the McArthur Basin, demonstrates that this unit is not homogeneous. As expected, the

formation is significantly thicker in sub-basins compared to paleohighs ([Figs. 8 and 12](#)). The undifferentiated Barney Creek Formation shows lateral facies variation. On the paleohigh in Lamont Pass 3, the undifferentiated Barney Creek Formation comprises carbonate facies deposited in shallow marine environments. In contrast, both the sub-basin intersection in GRNT-79-7 and the paleohigh intersection in Leila Yard 1 record deep subtidal and more siliciclastic-rich facies ([Fig. 8](#)).

The sedimentology of the HYC Pyritic Shale Member, which hosts the mineralization at McArthur River and Teena, is similar across the studied area and previously studied mineralized and unmineralized cores ([Large et al., 1998](#); [Bull, 1998](#)). However, the well-developed

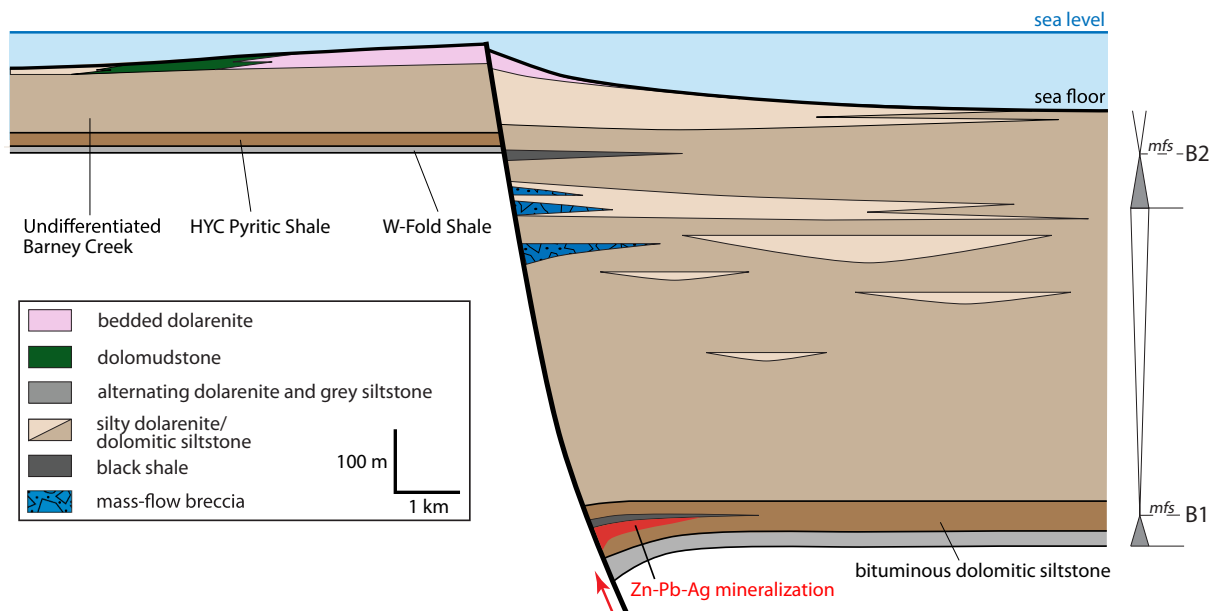


Fig. 12. Schematic cross-section illustrating the heterogeneity of the Barney Creek Formation in a paleohigh and sub-basin setting. Sequence stratigraphy is shown on the right. Note vertical exaggeration (1:10). Relative thickness changes are consistent with our core logs (see [Fig. 8](#)). In our preferred diagenetic model for mineralization, the MFS of sequence B1 would act as seal to ascending metalliferous fluids where it is developed as silty and black shale. In the syngenetic model (not shown) the black shale itself would be mineralized as it is more pyritic and organic-matter rich than the underlying transgressive sediments.

organic-rich and pyritic black shale and silty shale interval (MFS of sequence B1) in the sub-basin in GRNT-79-7 may be an important difference to paleohigh settings. Metallogenic models for McArthur-type deposits suggest metal transport by oxidized and sulfide-poor fluids, and chemical trapping by reducing and sulfidic strata (e.g., Large et al., 1998; Huston et al., 2006); the high abundance of organic matter and sulfide in the HYC Pyritic Shale Member would provide excellent trapping conditions. As the black shale interval in sub-basins is even more pyritic and organic-matter rich, it represents an even better chemical trap. This interval would therefore be the most prospective base metal target if the mineralization was syngenetic (Large et al., 1998). However, recent microcharacterization revealed that the mineralization at McArthur River occurred during late-stage diagenesis (Spinks et al., 2017). This model implies that mineralization occurred after initial compaction and lithification, which would have significantly reduced the initially high porosity and permeability of the black shale interval. Although developed as ideal chemical trap, the lithification and compaction would potentially convert the black shale interval into a seal (i.e., physical trap) for ascending brines. Following the diagenetic model, targeting should focus on the transgressive interval of the HYC Pyritic Shale Member below the MFS. Regardless of whether the MFS was a chemical trap (syngenetic model) or a physical trap (diagenetic model), sequence stratigraphy is a powerful tool for targeting as it predicts the stratigraphic position of this important interval. Ideally, it should be coupled to facies maps showing where in the basin the MFS is developed as a silty and black shale.

The alternatives of syngenetic and late-stage diagenetic mineralization have important implications for the timing of fluid pumping. Assuming syngenetic mineralization, Garven et al. (2001) linked fluid pumping to tectonic activity during deposition of the HYC Pyritic Shale Member. However, modeling by Sheldon and Schaub (2017) demonstrated that extension, which created the accommodation space for deposition of the HYC Pyritic Shale Member (e.g., McGoldrick et al., 2010), does not promote upward fluid flow. The diagenetic model implies that fluid pumping occurred later during undifferentiated Barney Creek time. A suitable stratigraphic interval might be the upper Barney Creek Formation around the B1–B2 sequence boundary. Here mass-flow breccias are common (Fig. 8). Although speculative, they may record slope and platform failure caused by a short-lived compressional event. This would be consistent with observations from the McArthur River deposit, where Hinman (1995) postulated compression during deposition of the upper Barney Creek Formation. This compressional event could be a suitable fluid pumping mechanism in the diagenetic model.

The generally lower abundance of organic matter and sulfide as reductant and possible sulfur source in the undifferentiated Barney Creek Formation has a negative effect on the trapping potential. This makes this part of the Barney Creek Formation less attractive than the HYC Pyritic Shale Member. An exception could be the organic-rich and pyritic black shale interval developed at the MFS of sequence B2 in the sub-basin section in GRNT-79-7 (Figs. 9 and 12). However, as the host unit and its trapping potential is only one critical component of the mineral system, other components (e.g., fluid pumping) also need to be considered. The same is true for the lower Caranbirini Member, which shows good trapping potential due to the organic-rich and pyritic composition of the recorded MFS of sequence L (Fig. 8).

6. Conclusion

A facies analysis reveals that rocks of the middle McArthur Group (i.e., Tooganinie to Lynott Formation) can be grouped into four facies associations and 19 lithofacies, spanning diverse depositional environments from deep subtidal and slope to supratidal sabkhas. Based on this

detailed sedimentological evaluation, we provide a sequence stratigraphic interpretation of the middle McArthur Group. Confirming Bull (1998), the Barney Creek Formation and overlying Reward Dolostone comprise two T-R sequences. This observation can be used to distinguish the Barney Creek Formation from the lithologically similar Caranbirini Member, which only consists of one incomplete sequence. The middle McArthur Group shows a systematic 3.5‰ $\delta^{13}\text{C}_{\text{carb}}$ trend that does not correspond to variation in depositional environments and thus likely reflects a basin-wide signal. In contrast, 1–2‰ variation in the Barney Creek Formation and Reward Dolostone correspond to changes in relative water depth and likely represent an isotope gradient within the basin. We use our sequence stratigraphic interpretation of the middle McArthur Group in the southern McArthur Basin to propose a possible correlation with coeval strata from the Lawn Hill Platform in Queensland. Furthermore, based on strikingly similar $\delta^{13}\text{C}_{\text{carb}}$ records and comparable ages, we propose that the middle McArthur Group correlates with the Tuanshanzi Formation from the North China Craton.

Important for mineral exploration, our study shows that the Barney Creek Formation is a heterogeneous unit. As generally agreed, the HYC Pyritic Shale Member is most prospective in sub-basins where it is thicker. In the depocenters of sub-basins, a maximum flooding surface in the HYC Pyritic Shale Member is developed as pyritic and organic-rich silty shale and black shale. If the mineralization was syngenetic, this interval would be an ideal chemical trap for base metal mineralization. In contrast, in the diagenetic model for mineralization, it would likely be a physical trap (seal) for ascending metalliferous brines due to compaction and lithification. Regardless of the preferred model for mineralization, sequence stratigraphy can be used to target this interval, ideally combined with facies maps depicting the lithological variation of this maximum flooding surface within the basin.

Acknowledgments

We acknowledge support by staff from the NT Geological Survey core store who lifted more than 1000 core trays. Hao Bui analyzed all carbon and oxygen isotope samples, which is much appreciated. We thank Rodney King (Teck Resources) and Alan Collins (University of Adelaide) for encouraging discussions. Associate editor Ignacio González-Álvarez invited us to contribute to this special issue and provided excellent editorial guidance. The feedback from Malcolm Wallace and an anonymous reviewer helped us to significantly improve the science, clarity, and focus of the paper. We thank many colleagues from CSIRO and the NT Geological Survey, namely Peter Schaub, Sam Spinks, Tim Munday, Heather Sheldon, Clive Foss, Tim Munson, Matt McGloin, Dot Close, Andrew Wygralak, and Louise Fisher. We are grateful to CSIRO Mineral Resources and the NT Geological Survey for funding this project. MK and TNB publish with permission of the Executive Director of the NT Geological Survey.

Appendix A. Supplementary data

Supplementary data associated with this article can be found, in the online version, at <https://doi.org/10.1016/j.oregeorev.2019.01.011>.

References

- Ahmad, M., Dunster, J.N., Munson, T.J., 2013. McArthur Basin. In: Ahmad, M., Munson, T.J. (Eds.), *Geology and mineral resources of the Northern Territory. Special Publication 5. Northern Territory Geological Survey* pp. 15:1–15:72.
- Allan, J.R., Matthews, R.K., 1982. Isotope signatures associated with early meteoric diagenesis. *Sedimentology* 29, 797–817.
- Alsharhan, A.S., Kendall, C.G.S.C., 2003. Holocene coastal carbonates and evaporites of the southern Arabian Gulf and their ancient analogues. *Earth-Sci. Rev.* 61, 1.
- Baruch, E.T., Kennedy, M.J., Löhr, S.C., Dewhurst, D.N., 2015. Feldspar dissolution-

- enhanced porosity in Paleoproterozoic shale reservoir facies from the Barney Creek Formation (McArthur Basin, Australia). *Am. Assoc. Pet. Geol. Bull.* 99 (9), 1745–1770.
- Bathurst, R.G.C., 1975. Carbonate Sediments and their Diagenesis. *Developments in Sedimentology*, No 12. Elsevier, Amsterdam.
- Betts, P.G., Giles, D., 2006. The 1800–1100 Ma tectonic evolution of Australia. *Precamb. Res.* 144, 92–125.
- Betts, P.G., Giles, D., Lister, G.S., 2003. Tectonic environment of shale-hosted massive sulfide Pb–Zn–Ag deposits of proterozoic Northeastern Australia. *Econ. Geol.* 98, 557–576.
- Blaikie, T.N., Kunzmann, M., 2018. Understanding the architecture of the Batten Fault Zone from the regional to sub-basin scale. Insights from geophysical interpretation and modelling. In: AGES 2018 Proceedings. Northern Territory Geological Survey, pp. 58–61.
- Bradshaw, B.E., Lindsay, J.F., Krassay, A.A., Wells, A.T., 2000. Attenuated basin-margin sequence stratigraphy of the Palaeoproterozoic Calvert and Isa Superbasins: the Fickling Group, southern Murphy Inlier, Queensland. *Aust. J. Earth Sci.* 47, 599–623.
- Brown, M.C., Claxton, C.W., Plumb, K.A., 1978. The Barney Creek Formation and some associated carbonate units of the McArthur Group. Northern Territory. Bureau of Mineral Resources Record 1969/145. 59p.
- Bull, S.W., 1998. Sedimentology of the Palaeoproterozoic Barney Creek Formation in DDH BMR McArthur 2, southern McArthur Basin, northern Territory. *Aust. J. Earth Sci.* 45, 21–31.
- Butler, G.P., 1969. Modern evaporite deposition and geochemistry of coexisting Brines, the Sabkha, Trucial Coast, Arabian Gulf. *J. Sediment. Petrol.* 39 (1), 70–89.
- Chen, J., Walter, M.R., Logan, G.A., Hinman, M.C., Summons, R.E., 2003. The Paleoproterozoic McArthur River (HYC) Pb/Zn/Ag deposit of northern Australia: organic geochemistry and ore genesis. *Earth Planet. Sci. Lett.* 210, 467–479.
- Chu, X., Zhang, T., Zhang, Q., Lyons, T.W., 2007. Sulfur and carbon isotope records from 1700 to 800 Ma carbonates of the Jixian section, northern China: implications for secular isotope variations in Proterozoic seawater and relationships to global supercontinental events. *Geochim. Cosmochim. Acta* 71, 4668–4692.
- Coniglio, M., Dix, G.R., 1992. Carbonate slopes. In: Walker, R.G., James, N.P. (Eds.), *Facies Models: Response to Sea Level Change*. Geological Society of Canada, pp. 349–373.
- Cook, H.E., Mullins, H.T., 1983. Basin margin environment. In: Scholle, P.A., Bebout, D.G., Moore, C.H. (Eds.), *Carbonate Depositional Environments*. AAPG Memoir 33, American Association of Petroleum Geologists, pp. 540–617.
- Cox, G.M., Halverson, G.P., Stevenson, R.S., Vokaty, M., Poirier, A., Kunzmann, M., Li, Z.-X., Dudas, F.Ö., Strauss, J.V., Macdonald, F.A., 2016. Continental flood basalt weathering as a trigger for Neoproterozoic Snowball Earth. *Earth Planet. Sci. Lett.* 446, 89–99.
- Crick, I.H., Boreman, C.J., Cook, A.C., Powell, T.G., 1988. Petroleum Geology and Geochemistry of Middle Proterozoic McArthur Basin, Northern Australia II: assessment of source rock potential. *Am. Assoc. Pet. Geol. Bull.* 72, 1495–1514.
- Croxford, N.J.W., 1975. The McArthur deposit: a review of the current situation. *Miner. Depos.* 10, 302–304.
- Davidson, G.J., Dashlooty, S.A., 1993. The Glyde Sub-basin: a volcanoclastic-bearing pull-apart basin coeval with the McArthur River base-metal deposit, Northern Territory. *Aust. J. Earth Sci.* 40 (6), 527–543.
- de la Rocha, C.L., 2006. The biological pump. In: Elderfield, H. (Ed.), *The Oceans and Marine Geochemistry*. Treatise in Geochemistry, vol. 6 Pergamon.
- Dill, R.F., Shinn, E.A., Jones, A.T., Kelly, K., Steinen, R.P., 1986. Giant subtidal stromatolites forming in normal salinity waters. *Nature* 324, 55–58.
- Dravis, J.J., 1983. Hardened subtidal stromatolites, Bahamas. *Science* 219, 385–386.
- Duane, M.J., Al-Zamel, A.Z., 1999. Syngenetic textural evolution of modern Sabkha stromatolites (Kuwait). *Sed. Geol.* 127, 237–245.
- Eldridge, C.S., Williams, N., Walshe, J.L., 1992. Sulfur isotope variability in sediment-hosted massive sulfide deposits as determined using ion microprobe SHRIMP: II. A Study of the H.Y.C. Deposit at McArthur River, Northern Territory, Australia. *Econ. Geol.* 88, 1–26.
- Embry, A.F., 1993. Transgressive–regressive (T–R) sequence analysis of the Jurassic succession of the Sverdrup Basin, Canadian Arctic Archipelago. *Can. J. Earth Sci.* 30, 301–320.
- Embry, A.F., 2009. Practical sequence stratigraphy. *Can. Soc. Petrol. Geol.*
- Embry, A.F., Johannessen, E.P., 2017. Two approaches to sequence stratigraphy. In: Montenari, M. (Ed.), *Stratigraphy and Timescales*. Advances in Sequence Stratigraphy, vol. 2. Elsevier, pp. 85–118.
- Evans, G., Schmidt, V., Bush, P., Nelson, H., 1969. Stratigraphy and geologic history of the sabkha, Abu Dhabi, Persian Gulf. *Sedimentology* 12, 145–159.
- Field, R.M., 1931. Geology of the Bahamas. *Geol. Soc. Am. Bull.* 42, 759–784.
- Flügel, E., 2004. *Microfacies of Carbonate Rocks – Analysis, Interpretation and Application*. Springer, Berlin.
- Garven, G., Bull, S.W., Large, R.R., 2001. Hydrothermal fluid flow models of stratiform ore genesis in the McArthur Basin, Northern Territory, Australia. *Geofluids* 1, 289–311.
- Gibson, G.M., Hutton, L.J., Holzschuh, J., 2017. Basin inversion and supercontinent assembly as drivers of sediment-hosted Pb–Zn mineralization in the Mount Isa region, northern Australia. *J. Geol. Soc.* 174, 773–786.
- Giles, D., Betts, P.G., Lister, G., 2002. Far-field continental backarc setting for the 1.80–1.67 Ga basins of northeastern, Australia. *Geology* 30 (9), 823–826.
- Halley, R.B., Harris, P.M., Hine, A.C., 1983. Bank margin environment. In: Scholle, P.A., Bebout, D.G., Moore, C.H. (Eds.), *Carbonate Depositional Environments*. AAPG Memoir 33, American Association of Petroleum Geologists, pp. 464–506.
- Halverson, G.P., 2013. Marine isotope stratigraphy. In: *Encyclopedia of Scientific Dating Methods*. Springer.
- Halverson, G.P., Hoffman, P.F., Schrag, D.P., Maloof, A.C., Rice, A.H.N., 2005. Towards a Neoproterozoic composite carbon isotope record. *Geol. Soc. Am. Bull.* 117, 1181–1207.
- Halverson, G.P., Wade, B.P., Hurtgen, M.T., Barovich, K.M., 2010. Neoproterozoic chemostratigraphy. *Precamb. Res.* 182, 337–350.
- Hine, A.C., 1977. Lily Bank, Bahamas: history of an active oolite sand shoal. *J. Sediment. Petrol.* 47 (4), 1554–1581.
- Hinman, M., 1995. Structure and kinematics of the HYC–Cooley Zone at McArthur River (Tech. rep.). Australian Geological Survey Organisation.
- Hodgskiss, M.S.W., Kunzmann, M., Poirier, A., Halverson, G.P., 2018. The role of microbial iron reduction in the formation of Proterozoic molar tooth structures. *Earth Planet. Sci. Lett.* 482, 1–11.
- Hoefs, J., 2009. *Stable Isotope Geochemistry*. Springer.
- Hoffman, P.F., 1976. Stromatolite morphogenesis in Shark Bay, Western Australia. In: Walter, M.R. (Ed.), *Developments in Sedimentology: Stromatolites*, vol. 20. Elsevier, Amsterdam, pp. 261–271.
- Hoffman, P.F., Halverson, G.P., Domack, E.W., Husson, J.M., Higgins, J.A., Schrag, D.P., 2007. Are basal Ediacaran (635 Ma) post-glacial cap dolostones diachronous? *Earth Planet. Sci. Lett.* 258, 114–131.
- Holman, A.L., Grice, K., Jaraula, C.M.B., Schimmelmann, A., 2014. Bitumen II from the Paleoproterozoic Here's Your Chance Pb/Zn/Ag deposit: implications for the analysis of depositional environment and thermal maturity of hydrothermally-altered sediments. *Geochim. Cosmochim. Acta* 139, 98–109.
- Huston, D.L., Stevens, B., Southgate, P.N., Muhling, P., Wyborn, L., 2006. Australian Zn–Pb–Ag ore-forming systems: a review and analysis. *Econ. Geol.* 101, 1117–1157.
- Illing, L.V., 1954. Bahaman calcareous sands. *Am. Assoc. Pet. Geol. Bull.* 38, 1–95.
- Inden, R.F., Moore, C.H., 1983. Beach environment. In: Scholle, P.A., Bebout, D.G., Moore, C.H. (Eds.), *Carbonate Depositional Environments*. AAPG Memoir 33, American Association of Petroleum Geologists, pp. 212–265.
- Ireland, T., Bull, S.W., Large, R.R., 2004a. Mass-flow sedimentology within the HYC Zn–Pb–Ag deposit, Northern Territory, Australia: evidence for syn-sedimentary ore genesis. *Miner. Depos.* 39, 143–158.
- Ireland, T., Large, R.R., McGoldrick, P., Blake, M., 2004b. Spatial distribution patterns of sulfur isotopes, nodular carbonate, and ore textures in the McArthur River (HYC) Zn–Pb–Ag Deposit, Northern Territory, Australia. *Econ. Geol.* 99, 1687–1709.
- Jackson, M.J., Powell, T.G., Summons, R.E., Sweet, I.P., 1986. Hydrocarbon shows and petroleum source rocks in sediments as old as 1.7×10^9 years. *Nature* 322, 727–729.
- Jackson, M.J., Muir, M.D., Plumb, K.A., 1987. Geology of the southern McArthur Basin, Northern Territory. Bureau Min. Resour. Bull. 220, 315.
- Jackson, M.J., Sweet, I.P., Powell, T.G., 1988. Studies on petroleum geology and geochemistry, middle Proterozoic McArthur Basin, Northern Australia I: petroleum potential. *Austr. Petrol. Exploration J.* 28, 283–302.
- Jackson, M.J., Southgate, P.N., Winefield, P.R., Barnett, K., Zeilinger, I., 2000. Revised sub-division and regional correlation of the McArthur Basin succession based on NABRE's 1995–8 sequence stratigraphic studies. *AGSO Record* 2000/3. 79pp.
- Jahnert, R.J., Collins, L.B., 2011. Significance of subtidal microbial deposits in Shark Bay, Australia. *Mar. Geol.* 286, 106–111.
- Jahnert, R.J., Collins, L.B., 2012. Characteristics, distribution and morphogenesis of subtidal microbial systems in Shark Bay, Australia. *Mar. Geol.* 303–306, 115–136.
- James, N.P., Jones, B., 2016. *Origin of Carbonate Sedimentary Rocks*. Wiley.
- Kendall, C.G.S.C., Alsharhan, A.S., 2011. Holocene geomorphology and recent carbonate–evaporite sedimentation of the coastal region of Abu Dhabi, United Arab Emirates. *Int. Assoc. Sedimentol. Spec. Publ.* 43, 45–88.
- Kendall, C.G.S.C., Skipwith, P.A., 1968. Recent algal mats of a Persian Gulf lagoon. *J. Sed. Petrol.* 38 (4), 1040–1058.
- Kendall, C.G.S.C., Skipwith, P.A., 1969a. Geomorphology of a Recent Shallow-Water Carbonate Province: Khor al Bazam, Trucial Coast, Southwest Persian Gulf. *Geol. Soc. Am. Bull.* 80, 865–892.
- Kendall, C.G.S.C., Skipwith, P.A., 1969b. Holocene Shallow-Water Carbonate and Evaporite Sediments of Khor Al Bazam, Abu Dhabi, Southwest Persian Gulf. *Am. Assoc. Pet. Geol. Bull.* 53 (4), 841–869.
- Kendall, C.G.S.C., Warren, J.K., 1987. A review of the origin and setting of tepees and their associated fabrics. *Sedimentology* 34, 1007–1027.
- Kinsman, D.J.J., Park, R.K., 1976. Algal belt and coastal sabkha evolution, Trucial Coast, Persian Gulf. In: In: Walter, M. (Ed.), *Developments in Sedimentology: Stromatolites*, vol. 20. Elsevier, Amsterdam, pp. 421–433.
- Kirkham, A., 1997. Shoreline evolution, aeolian deflation and anhydrite distribution of the Holocene, Abu Dhabi. *GeoArabia* 2 (4), 403–416.
- Krassay, A.A., Bradshaw, B.E., Domagala, J., Jackson, M.J., 2000. Siliciclastic shoreline to growth-faulted, turbiditic sub-basins: the Proterozoic River Supersequence of the upper McNamara Group on the Lawn Hill Platform, Northern Australia. *Aust. J. Earth Sci.* 47, 533–562.
- Kump, L., Arthur, M.A., 1999. Interpreting carbon-isotope excursions: carbonates and organic matter. *Chem. Geol.* 161 (1–3), 181–198.
- Kunzmann, M., Gutzmer, J., Beukes, N.J., Halverson, G.P., 2014. Depositional environment and lithostratigraphy of the Paleoproterozoic Mooidraai Formation, Kalahari

- Manganese Field, South Africa. *S. Afr. J. Geol.* 117 (2), 173–192.
- Lambert, I.B., Scott, K.M., 1973. Implications of geochemical investigations of sedimentary rocks within and around the McArthur zinc-lead-silver deposit, Northern Territory. *J. Geochem. Explor.* 2, 307–330.
- Large, R.R., Bull, S.W., Cooke, D.R., McGoldrick, P.J., 1998. A genetic model for the HYC deposit, Australia: based on regional sedimentology, geochemistry, and sulfide-sediment relationships. *Econ. Geol.* 93, 1345–1368.
- Leach, D.L., Sangster, D.F., Kelley, K.D., Large, R.R., Garven, G., Allen, C.R., Gutzmer, J., Walters, S., 2005. Sediment-hosted lead-zinc deposits: a global perspective. *Economic Geology 100th Anniversary Volume*. pp. 561–607.
- Leach, D.L., Bradley, D.C., Huston, D.L., Pisarevsky, S.A., Taylor, R.D., Gardoll, S.J., 2010. Sediment-hosted lead-zinc deposits in earth history. *Econ. Geol.* 105, 593–625.
- Lindsay, J.F., Brasier, M.D., 2000. A carbon isotope reference curve for ca. 1700–1575 Ma, McArthur and Mount Isa Basins, Northern Australia. *Precamb. Res.* 99, 271–308.
- Logan, B.W., 1961. Cryptozoan and associated stromatolites from the Recent, Shark Bay, Western Australia. *J. Geol.* 69 (5), 517–533.
- Logan, B.W., Rezak, R., Ginsburg, R.N., 1964. Classification and environmental significance of algal stromatolites. *J. Geol.* 72 (1), 68–83.
- Logan, R.G., Murray, W.J., Williams, N., 1990. HYC silver-lead-zinc deposit, McArthur River. In: Hughes, F.F. (Ed.), *Geology of the Mineral Deposits of Australia and Papua New Guinea*. The Australasian Institute of Mining and Metallurgy, vol. 1. pp. 907–911.
- Logan, G.A., Hinman, M.C., Walter, M.R., Summons, R.E., 2001. Biogeochemistry of the 1640 Ma McArthur River (HYC) lead-zinc ore and host-sediments, Northern Territory, Australia. *Geochim. Cosmochim. Acta* 65 (14), 2317–2336.
- Lu, S.N., Li, H.M., 1991. A precise U-Pb single zircon age determination for the volcanics of the Dahongyao Formation, Changcheng System in Jixian. *Bull. Chin. Acad. Geol. Sci.* 22, 137–145.
- Lu, S.N., Zhao, G.C., Wang, H.M., Hao, G.J., 2008. Precambrian metamorphic basement and sedimentary cover of the North China Craton: a review. *Precamb. Res.* 160, 77–93.
- Macdonald, F.A., Strauss, J.V., Sperling, E.A., Halverson, G.P., Narbonne, G.M., Johnston, D.T., Kunzmann, M., Schrag, D.P., Higgins, J.A., 2013. The stratigraphic relationship between the Shuram carbon isotope excursion, the oxygenation of Neoproterozoic oceans, and the first appearance of the Ediacara biota and bilaterian trace fossils in northwestern Canada. *Chem. Geol.* 362, 250–272.
- Maloof, A.C., Grotzinger, J.P., 2012. The Holocene shallowing-upward parasequence of north-west Andros Island, Bahamas. *Sedimentology* 59, 1375–1407.
- Maslin, M.A., Swann, G.E.A., 2005. Isotopes in marine sediments. In: Leng, M.J. (Ed.), *Isotopes in Palaeoenvironmental Research*. Springer.
- McGoldrick, P.J., Winefield, P., Bull, S.W., Selley, D., Scott, R., 2010. Sequences, syndimentary structures, and sub-basins: the where and when of SEDEX zinc systems in the Southern McArthur Basin, Australia. *Soc. Econ. Geol. Spec. Publ.* 15, 367–389.
- Meng, Q.-R., Wei, H.-H., Qu, Y.-Q., Ma, S.-X., 2011. Stratigraphic and sedimentary records of the rift to drift evolution of the northern North China craton at the Paleoproterozoic transition. *Gondwana Res.* 20, 205–218.
- Nystuen, J.P., 1998. History and development of sequence stratigraphy. In: Gradstein, F.M., Sandvik, K.O., Milton, N.J. (Eds.), *Sequence Stratigraphy – Concepts and Applications*. Norwegian Petroleum Society, Special Publications 8, Amsterdam. pp. 31–116.
- Page, R.W., Sweet, I.P., 1998. Geochronology of basin phases in the western Mt Isa Inlier, and correlation with the McArthur Basin. *Aust. J. Earth Sci.* 45, 219–232.
- Page, R.W., Jackson, M.J., Krassay, A.A., 2000. Constraining sequence stratigraphy in north Australian basins: SHRIMP U-Pb zircon geochronology between Mt Isa and McArthur River. *Aust. J. Earth Sci.* 47, 431–459.
- Park, R.K., 1977. The preservation potential of some Recent stromatolites. *Sedimentology* 24, 485–506.
- Playford, P.E., Cockbain, A.E., Berry, P.F., Roberts, A.P., Haines, P.W., Brooke, B.P., 2013. The Geology of Shark Bay. *Geol. Survey Western Austr. Bull.* 146, 281.
- Playton, T.E., Janson, X., Kerans, C., 2010. Carbonate slopes. In: James, N.P., Dalrymple, R.W. (Eds.), *Facies Models 4*. Geological Association of Canada, pp. 449–476.
- Plint, A.G., 1988. Sharp-based shoreface sequences and “offshore bars” in the Cardium Formation of Alberta: their relationship to relative changes in sea level. In: *Sea-Level Changes – An Integrated Approach*. Vol. SEPM Special Publication 42. The Society of Economic Paleontologists and Mineralogists.
- Plumb, K.A., 1979a. Structure and tectonic style of the Precambrian shields and platforms of northern Australia. *Tectonophysics* 58, 291–325.
- Plumb, K.A., 1979b. The tectonic evolution of Australia. *Earth Sci. Rev.* 14, 205–249.
- Plumb, K.A., Brown, M.C., 1973. Revised correlations and stratigraphic nomenclature in the Proterozoic carbonate complex of the McArthur Group, Northern Territory. *Bureau Min. Resour. Bull.* 139, 103–115.
- Plumb, K.A., Wellman, P., 1987. McArthur Basin, Northern Territory: mapping of deep troughs using gravity and magnetic anomalies. *BMR J. Geol. Geophys.* 10, 243–251.
- Porter, T.M., 2017. McArthur River Zn-Pb-Ag deposit. In: Phillips, N. (Ed.), *Australian Ore Deposits*. AusIMM Monograph 32. pp. 479–482.
- Rankey, E.C., 2002. Spatial patterns of sediment accumulation on a Holocene carbonate tidal flat, northwest Andros Island, Bahamas. *J. Sediment. Res.* 72 (5), 591–601.
- Rankey, E.C., Morgan, J., 2002. Quantified rates of geomorphic change on a modern carbonate tidal flat, Bahamas. *Geology* 30 (7), 583–586.
- Rankey, E.C., Reeder, S.L., 2011. Holocene oolitic marine sand complexes of the Bahamas. *J. Sediment. Res.* 81, 97–117.
- Rankey, E.C., Riegl, B., Steffen, K., 2006. Form, function and feedbacks in a tidally dominated ooid shoal, Bahamas. *Sedimentology* 53, 1191–1210.
- Rawlings, D.J., 1999. Stratigraphic resolution of a multiphase intracratonic basin system: the McArthur Basin, northern Australia. *Aust. J. Earth Sci.* 46, 703–723.
- Rawlings, D.J., Korsch, R.J., Goleby, G.M., Gibson, G.M., Johnstone, D.W., Barlow, M., 2004. The 2002 Southern McArthur Basin Seismic Reflection Survey. *Geoscience Australia Record* 2004/17. 78p.
- Reeder, S.L., Rankey, E.C., 2008. Interactions between tidal flows and ooid shoals, northern Bahamas. *J. Sediment. Res.* 78, 175–186.
- Reid, R.P., James, N.P., Macintyre, I.G., Dupraz, C.P., Burne, R.V., 2003. Shark Bay stromatolites: microfabrics and reinterpretation of origins. *Facies* 49, 299–324.
- Reijmer, J.J.G., Swart, P.K., Bauch, T., Otto, R., Reuning, L., Roth, S., Zechel, S., 2009. A re-evaluation of facies on Great Bahama Bank I: new facies maps of western Great Bahama Bank. *Int. Assoc. Sedimentol. Spec. Publ.* 41, 29–46.
- Saltzman, M.R., Thomas, E., 2012. Carbon isotope stratigraphy. In: Gradstein, F.M., Ogg, J.G., Schmitz, M., Ogg, G. (Eds.), *The Geologic Time Scale*. Elsevier.
- Sarmiento, J.L., Gruber, N., 2006. *Ocean Biogeochemical Dynamics*. Princeton University Press.
- Schmid, S., 2017. Neoproterozoic evaporites and their role in carbon isotope chemotratigraphy (Amadeus Basin, Australia). *Precamb. Res.* 290, 16–31.
- Scott, D.L., Rawlings, D.J., Page, R.W., Tarlowski, C.Z., Idnurm, M., Jackson, M.J., Southgate, P.N., 2000. Basement framework and geodynamic evolution of the Palaeoproterozoic superbasins of north-central Australia: an integrated review of geochemical, geochronological and geophysical data. *Aust. J. Earth Sci.* 47, 341–380.
- Selway, K., Hand, M., Heinsohn, G.S., Payne, J.L., 2009. Magnetotelluric constraints on subduction polarity reversal: reversing reconstruction models for Proterozoic Australia. *Geology* 37 (9), 799–802.
- Sheldon, H.A., Schaubs, P.M., 2017. Investigating controls on mineralisation in the Batten Fault Zone using numerical models. In: *Annual Geoscience Exploration Seminar Proceedings*. Northern Territory Geological Survey, pp. 67–71.
- Shinn, E.A., 1968. Practical significance of birdseye structures in carbonate rocks. *J. Sed. Petrol.* 38 (1), 215–223.
- Shinn, E.A., 1983a. Birdseyes, fenestrae, shrinkage pores, and loferites: a reevaluation. *J. Sed. Petrol.* 53 (2), 619–628.
- Shinn, E.A., 1983b. Tidal flat environments. In: Scholle, P.A., Bebout, D.G., Moore, C.H. (Eds.), *Carbonate Depositional Environments*. AAPG Memoir 33, American Association of Petroleum Geologists, pp. 172–210.
- Shinn, E.A., Robbin, D.M., 1983. Mechanical and chemical compaction in fine-grained shallow-water limestones. *J. Sediment. Petrol.* 53 (2), 595–618.
- Shinn, E.A., Llyod, R.M., Ginsburg, R.N., 1969. Anatomy of a modern carbonate tidal-flat: Andros Island, Bahamas. *J. Sediment. Res.* 39 (3), 1202–1228.
- Smith, J.W., Croxford, N.J.W., 1973. Sulphur Isotope Ratios in the McArthur Lead-Zinc-Silver Deposit. *Nature* 245, 10–12.
- Smith, J.W., Croxford, N.J.W., 1975. An isotopic investigation of the environment of deposition of the McArthur mineralization. *Miner. Depos.* 10, 269–276.
- Smith, E.F., Macdonald, F.A., Petach, T.A., Bold, U., Schrag, D.P., 2016. Integrated stratigraphic, geochemical, paleontological stratigraphic late Ediacaran to early Cambrian records from southwestern Mongolia. *Geol. Soc. Am. Bull.* 128 (3–4), 442–468.
- Southgate, P.N., Bradshaw, B.E., Domagala, J., Jackson, M.J., Idnurm, M., Krassay, A.A., Page, R.W., Sami, T.T., Scott, D.L., Lindsay, J.F., McConachie, B.A., Tarlowski, C., 2000. Chronostratigraphic basin framework for Palaeoproterozoic rocks (1730–1575 Ma) in northern Australia and implications for base-metal mineralisation. *Aust. J. Earth Sci.* 47, 461–483.
- Spinks, S.A., Schmid, S., Pagés, A., Bluett, J., 2016. Evidence for SEDEX-style mineralization in the 1.7 Ga Tawallah Group, McArthur Basin, Australia. *Ore Geol. Rev.* 76, 122–139.
- Spinks, S., Pearce, M., Ryan, C., Kunzmann, M., Fisher, L., 2017. Finally mapping thallium: evidence for a diagenetic origin for a classic sedimentary ‘exhalative’ Zn-Pb deposit? In: *Resources for Future Generations*, Abstract 2345.
- Stiller, M., Rounick, J.S., Sasha, S., 1985. Extreme carbon-isotope enrichments in evaporating brines. *Nature* 316, 434–435.
- Summons, R.E., Powell, T.G., Boreham, C.J., 1988. Petroleum geology and geochemistry of the Middle Proterozoic McArthur Basin, Northern Australia: III. Composition of extractable hydrocarbons. *Geochim. Cosmochim. Acta* 52, 1747–1763.
- Suosaari, E.P., Reid, R.P., Palford, P.E., Foster, J.S., Stolz, J.F., Casaburi, G., Hagan, P.D., Chirayath, V., Macintyre, I.G., Planavsky, N.J., Eberli, G.P., 2016. New multi-scale perspectives on the stromatolites of Shark Bay, Western Australia. *Scientific Rep.* 6, 20557. <https://doi.org/10.1038/srep20557>.
- Symons, D.T.A., 2006. HYC (McArthur River) SEDEX deposit, Australia: First paleomagnetic results. *J. Geochem. Explor.* 89, 380–383.
- Taylor, M.L., McMillan, N.E., Dalrymple, L.J., Hayward, N., 2017. Teena zinc-lead deposit. In: Phillips, N. (Ed.), *Australian Ore Deposits*. AusIMM Monograph 32, pp. 483–484.
- Vail, P.R., Audemard, F., Bowman, S.A., Eisner, P.N., Perez-Cruz, C., 1991. The stratigraphic signatures of tectonics, eustasy and sedimentology. In: Einsele, G., Ricken, W., Seilacher, A. (Eds.), *Cycles and Events in Stratigraphy*. Springer, Berlin, pp. 617–659.
- Wagner, C.W., van der Togt, C., 1973. Holocene sediment types and their distribution in the southern Persian Gulf. In: Purser, B.H. (Ed.), *The Persian Gulf: Holocene Sediment Types and their Distribution in the Southern Persian Gulf*. Springer, pp. 123–155.

- Walker, R.N., Muir, M.D., Diver, W.L., Williams, N., Wilkins, N., 1977. Evidence of major sulphate evaporite deposits in the Proterozoic McArthur Group, Northern Territory, Australia. *Nature* 265, 526–529.
- Walker, R.N., Gulson, B., Smith, J., 1983. The Coxco deposit – a proterozoic Mississippi valley-type deposit in the McArthur River District, Northern Territory, Australia. *Econ. Geol.* 78, 214–249.
- Warren, J.K., 2010. Evaporites through time: tectonic, climatic and eustatic controls in marine and nonmarine deposits. *Earth Sci. Rev.* 98, 217–268.
- Warren, J.K., Kendall, C.G.S.C., 1985. Comparison of sequences formed in Marine Sabkha (Subaerial) and Salina (Subaqueous) settings – modern and ancient. *Am. Assoc. Pet. Geol. Bull.* 69 (6), 1013–1023.
- Wignall, P.B., 1994. *Black Shales*. Oxford University Press.
- Williams, N., 1978. Studies of the base metal sulfide deposits at McArthur river, Northern Territory, Australia: I. The Cooley and Ridge deposits. *Econ. Geol.* 73, 1005–1035.
- Williams, N., Rye, D.M., 1974. Alternative interpretation of sulphur isotope ratios in the McArthur lead-zinc-silver deposit. *Nature* 247, 535–537.
- Winefield, P.R., 1999. Sedimentology and diagenesis of Late Palaeoproterozoic carbonates, southern McArthur Basin, northern Australia (Ph.D. thesis). University of Tasmania, Hobart.
- Winefield, P.R., 2000. Development of late Paleoproterozoic aragonite seafloor cements in the McArthur Group, northern Australia. In: Grotzinger, J.P., James, N.P. (Eds.), *Carbonate Sedimentation and Diagenesis in the Evolving Precambrian World*. SEPM Special Publication, pp. 145–159 67.
- Wright, V.P., 1984. Peritidal carbonate facies models: a review. *Geol. J.* 19, 309–325.
- Zhang, S.H., Zhao, Y., Hao, Y.E., Hu, J.M., Wu, F., 2013. New constraints on ages of the Chuanlinggou and Tuanshanzi formations of the Changcheng System in the Yan-Liao area in the northern North China Craton. *Acta Petrol. Sin.* 29 (7), 2481–2490.